International Journal of Heat and Mass Transfer 256 (2026) 127904

Contents lists available at ScienceDirect

International Journal of Heat and Mass Transfer

journal homepage: www.elsevier.com/locate/ijhmt

From design to operation: Integrated optimization of intermediate cycle heat exchange systems for aero engines

Weitong Liu [a,b], Guoqiang Xu [a,b], Yiang Liu [a,b], Xiuting Gu [a,b], Jiayang Wang [a,b], Jingzhi Zhang [c], Yanchen Fu [a,b,*]

[a] Research Institute of Aero-engine, Beihang University, Beijing 100191, China
[b] Tianmushan Laboratory, Hangzhou 310023, China
[c] School of Nuclear Science, Energy and Power Engineering, Shandong University, Jinan, Shandong 250061, China

ARTICLE INFO

Keywords:
Thermodynamic system
Multi-objective optimization
Thermal management
Aero engine

ABSTRACT

Advanced aero-engine thermal management systems increasingly rely on intermediate cycle heat exchange (ICHE) systems to enable safe and efficient heat transfer between fuel and high-temperature air. While the ICHE configuration offers significant safety and anti-coking advantages over direct-contact cooling, current research lacks a unified optimization framework that jointly addresses system weight and thermal performance in design, as well as thermal adaptability in operation. To fill this gap, this study develops an integrated optimization framework for ICHE systems in aero engines, encompassing both design-stage trade-offs and operational regulation. For system design, a coordinated multi-objective optimization model is constructed using total heat transfer area and system-equivalent thermal conductance as objectives, and solved via a hybrid algorithm combining genetic algorithms with gradient-based methods. The resulting Pareto front reveals the nonlinear coupling between weight and heat transfer performance, offering flexible design choices. For operational optimization, a transfer matrix-based model is developed for multi-branch ICHE configurations and experimentally validated using a platform with aviation kerosene, high-pressure water, and air. By adjusting the intermediate working fluid mass flow rate and its distribution, the system heat transfer rate is maximized, with results indicating the dominant role of mean temperature difference over thermal conductance. Operational optimization yields a 7.98% increase in heat transfer rate, demonstrating the framework's effectiveness. This work provides a comprehensive method for optimizing ICHE systems across the full engine lifecycle, offering valuable insights into high-efficiency, lightweight thermal management design and operation for next-generation aero engines.

1. Introduction

The key to achieving a performance leap in high thrust-to-weight ratio aero engines lies in overcoming the thermal load bottleneck by increasing the compressor pressure ratio and turbine inlet temperature. However, both measures significantly elevate the thermal load on high-temperature turbine components. From the perspective of thermal protection technology development in aero engines, enhancing the temperature tolerance of turbine materials is largely constrained by development cycles and technological maturity, making substantial breakthroughs difficult in the short term. Meanwhile, although advanced and more complex cooling structures have been explored, the improvements in cooling performance remain relatively limited [1,2]. As a result, alongside continued research into novel cooling architectures, researchers have proposed utilizing the heat sink of onboard fuel to cool high-temperature components [3] or air [4], such as Cooled Cooling Air (CCA) technology [5]. CCA technology involves installing a fuel–air heat exchanger (HEX) on the aero engine to enhance the cooling effectiveness of cooling air while simultaneously preheating the onboard fuel to facilitate subsequent combustion [6]. CCA technology has achieved widespread success in practical applications. It has been adopted in both the European NEWAC project (New Aero Engine Core concepts) [7] and the US adaptive versatile engine technology project [8]. The AL-31F engine is the first in-service engine to implement CCA technology [9], marking a significant milestone in its development.

However, the strategy of employing onboard fuel as a heat sink for direct heat exchange with high-temperature air is constrained by two critical technical challenges. The first pertains to the limitations imposed by coking kinetics. As a hydrocarbon, aviation fuel undergoes

* Corresponding author.
E-mail address: yanchenfu@buaa.edu.cn (Y. Fu).

https://doi.org/10.1016/j.ijheatmasstransfer.2025.127904
Received 6 August 2025; Received in revised form 18 September 2025; Accepted 26 September 2025
Available online 6 October 2025

Nomenclature

A	heat transfer area of HEX [m^2]
A_{total}	total heat transfer area [m^2]
A_0	nominal total heat transfer area [m^2]
a	coefficient in the Nusselt number correlation
b	coefficient in the Nusselt number correlation
C	coefficient in the Nusselt number correlation
c_p	isobaric specific heat capacity [J/(kg·K)]
d	hydraulic diameter [mm]
F	composite optimization objective
f	calculation coefficient
G	heat capacity flow rate [J/(K·s)]
h	heat transfer coefficient [W/(m^2·K)]
K	overall heat transfer coefficient [W/(m^2·K)]
KA	thermal conductance of HEX [W/K]
$(KA)_{sys}$	system-equivalent thermal conductance [W/K]
$(KA)_0$	nominal system-equivalent thermal conductance [W/K]
n	number of heat exchange units
Nu	Nusselt number
P	pressure [Pa]
Pr	Prandtl number
Q	heat transfer rate [kW]
Q_{equal}	system steady-state heat transfer rate [kW]
R	thermal resistance of HEX based on the inlet temperature difference [K/W]
R_{wall}	solid wall thermal resistance [K/W]
Re	Reynolds number
s	calculation coefficient
T	temperature [K]
T_{limit}	boiling point of the intermediate working fluid [K]
$T_{fuel,max}$	fuel maximum permissible temperature [K]
ΔT_m	mean temperature difference [K]
t	calculation coefficient

Greek symbols

α	intermediate parameter
β	intermediate parameter
λ	thermal conductivity [W/(m·K)]
μ	dynamic viscosity [μPa·s]
ω	weighting factor
ζ	intermediate working fluid flow distribution ratio

Subscripts

1	HEX-1
2	HEX-2
3	HEX-3
a	air
c	cold-side fluid
f	fuel
h	hot-side fluid
i	inner side
in	inlet
internal	internal nodes
max	maximum
min	minimum
out	outlet
o	outer side
w	intermediate working fluid

Abbreviation

AMTD	Arithmetic mean temperature difference
CCA	Cooled Cooling Air
CFD	Computational Fluid Dynamics
GA	Genetic Algorithm
HEX	Heat exchanger
ICHE	Intermediate cycle heat exchange
LMTD	Logarithmic mean temperature difference
NSGA-II	Non-dominated Sorting Genetic Algorithm II
PCHE	Printed Circuit Heat Exchanger
SABRE	Synergistic Air-Breathing Rocket Engine
TMS	Thermal Management System

rapid thermal oxidative coking under supercritical pressure conditions (>2.33 MPa) when the wall temperature exceeds 150 °C [10,11]. This phenomenon leads to a reduction in the effective flow passage area and a deterioration in heat transfer performance, thereby imposing strict constraints on the permissible wall temperature in HEX design and narrowing the operational stability margin of fuel–air HEXs. The second challenge concerns safety risks. In direct heat exchange configurations, structural or seal failure of the HEX may result in direct contact between fuel and high-temperature air, posing a serious risk of combustion or explosion and thereby threatening the safety of the aircraft [12,13]. To address these two technical challenges, the academic community has proposed the adoption of a third fluid indirect cooling configuration, introducing an intermediate cycle heat exchange (ICHE) system into the thermal management architecture of aero engines.

A secure and dependable third working fluid is employed in the ICHE system to indirectly exchange heat between the fuel and the high-temperature air via separate HEXs within the intermediate cycle [14,15]. While achieving the intended objectives of CCA technology, the ICHE system offers additional advantages in terms of thermal stability and system safety. By enabling heat exchange between the fuel and a high–specific heat capacity intermediate working fluid (e.g., water), the fuel-side wall temperature of the HEX is reduced due to the lower temperature of the intermediate working fluid compared to high-temperature air. This alleviates thermal oxidative coking of the fuel, thereby enhancing the operational margin and stability of the HEX. Furthermore, since the fuel exchanges heat with a safe and reliable intermediate medium, and the fuel–intermediate working fluid HEX can be installed away from the core engine, the overall safety of the engine thermal management system is significantly improved. Reaction Engines Limited proposed the Synergistic Air-Breathing Rocket Engine (SABRE) within the Skylon project [16,17], featuring an innovative ICHE system utilizing three separate HEXs. By introducing helium as a closed-loop working fluid, the system enables indirect heat transfer between hydrogen fuel and high-temperature gases. This design improves thermal efficiency while addressing hydrogen-related safety and material challenges [18]. Subsequent iterations such as SABRE-3 [19], SABRE-4 [20], and Scimitar [21] continued to adopt this intermediate-cycle architecture. Liu et al [22] investigated the effect of working conditions on an aero-engine thermal management system with intermediate circulation based on the heat current method. Cheng et al [23] introduced an indirect fuel cooling system for a hydrocarbon-fueled scramjet, employing liquid metal as the intermediate fluid, and evaluated its thermal performance. Zhang et al [24] also investigated the application of liquid metals in aero-engine thermal management. A multilevel heat exchange system using aviation kerosene, high-pressure water, and air was proposed by Liu et al [15], and they established a transfer matrix-based model to identify system heat transfer characteristics. Dang et al [3] investigated various configurations of a segmented cooling thermal management system based on a closed Brayton cycle, where the carbon dioxide served as an intermediate medium for engine

wall cooling and fuel preheating. Overall, considering multiple benefits of ICHE system, it is playing an increasingly vital role in aero-engine thermal management systems.

The application of ICHE systems in aero engines presents a challenging optimization problem that spans the entire flight envelope in both design and operation. Based on the characteristics of engine thermal management systems, this optimization problem can be decomposed into two categories: design optimization and operational optimization.

For design optimization, the ICHE system must strike a balance between overall weight and heat transfer capacity. Although a complex ICHE system enables multi-level cascade utilization of energy throughout the engine, thereby improving thermal efficiency, the inclusion of additional heat exchange components and fluid circuits inevitably increases system weight, which can negatively impact the thrust-to-weight ratio of the engine. Therefore, design optimization should comprehensively account for both system weight and heat transfer performance to achieve a synergistic balance between the two. In the ICHE system, optimizing weight can be viewed as optimizing the heat transfer area under a fixed material constraint. Fu et al [25] developed a mathematical model of the ICHE system to determine the intermediate working fluid parameters for achieving the minimum system heat transfer area. Liu et al [26] combined artificial neural networks (ANN) with the heat current method to establish an optimization model aimed at minimizing the total thermal conductance of HEXs (KA) within the system. They proposed that thermal conductance serves as a surrogate for heat transfer area (A), and thus optimizing it enables the optimization of system weight. Wen et al [27] used the improved genetic algorithm (GA) to optimize the weight of the hydrogen engine thermal management system integrated with the ICHE system. Sarkar and Bhattacharyya [28] conducted an analytical investigation into minimizing the total heat transfer area and conductance in heat pumps and irreversible refrigerators, and validated their findings through numerical simulations. The optimal allocation of heat transfer area for the endoreversible and irreversible Carnot cycles for refrigeration and air-conditioning plants was analytically derived by Chen et al [29].

For operational optimization, considering that the flight envelope of an aero engine encompasses various conditions such as takeoff, climb, and cruise [30,31], the ICHE system must adapt to changing thermal loads across these conditions. This requires the rational allocation of intermediate working fluid mass flow rate among different subsystems and the development of adaptive flow regulation strategies to achieve optimal heat transfer performance throughout the entire flight envelope. Liu et al [32] employed the pinch method to optimize the total net power output of a power generation thermal management system for a hydrogen-fueled turbojet engine. However, Rašković and Stoiljković [33] pointed out that the pinch method, being based on heat transfer analysis, is strongly limited by the existence of complex physical or chemical process units. In practical thermal systems, all processes are inherently irreversible, and this irreversibility is generally characterized by entropy generation [34,35]. Bejan et al [36,37] proposed using the minimization of entropy generation as an optimization criterion for thermal systems, leading to the development of entropy generation analysis methods. The core concept of this approach is to describe system irreversibility through entropy generation, under the assumption that minimizing irreversibility corresponds to optimal system performance. However, Klein and Reindl [38] found, in their application of the minimum entropy generation principle to optimize refrigeration cycles, that the condition of minimum entropy generation does not always correspond to maximum system performance. In addition, exergy analysis is also commonly employed in the optimization of thermal systems. Balli et al [39] conducted a comparative exergy analysis of the thermodynamic performance of a TF33 engine fueled by aviation kerosene and hydrogen, revealing that the exergy efficiency of the combustor decreased by 12.51% when hydrogen fuel was used. However, exergy analysis alone does not provide explicit optimization criteria for determining the optimal parameters of components with the highest exergy losses [40]. In recent years, Chen et al [41,42] proposed the heat current method for thermal system analysis and optimization. This method characterizes system behavior by formulating global constraint equations and allows for the formulation of optimization objectives tailored to practical requirements. What is particularly noteworthy is that the treatment of the overall heat transfer coefficient of HEXs (K) has become a critical factor determining the accuracy and efficiency of heat current method–based optimization [14]. Liu et al [43] employed the heat current method to optimize a multi-loop heat exchange system, achieving a 27% reduction in total pump power consumption. During the optimization process, they used Computational Fluid Dynamics (CFD) to iteratively calculate the overall heat transfer coefficient of the HEXs.

Nonetheless, current research falls short in achieving full-process optimization of ICHE systems, especially for aero engines where minimizing system weight and maximizing heat transfer capacity are critical to enhancing engine performance. Design-level optimization studies rarely address the simultaneous consideration of system weight and heat transfer capacity. Most studies isolate either weight or HEX thermal conductance, lacking mechanisms to balance the inherent trade-off between these factors. In terms of operational optimization, regulatory strategies for full-flight-envelope conditions remain underexplored. Furthermore, existing optimization methods lack efficiency and generalizability in computing the overall heat transfer coefficient.

This study develops a full-process optimization framework for ICHE systems in aero engines, encompassing both design and operational stages. In the design stage, a coordinated multi-objective optimization framework is formulated, targeting total heat transfer area and system-equivalent thermal conductance. A scalarized objective function is applied to derive the Pareto front, elucidating the trade-off between ICHE system weight and heat transfer performance. For operational optimization, a hybrid algorithm is employed to maximize the system heat transfer rate. An experimental platform employing aviation kerosene, air, and high-pressure water as working fluids is constructed. The proposed optimization model is validated through comparison with initial experimental data.

2. System description and experimental facility

2.1. Basic ICHE system

The schematic of the basic ICHE system for aero engines is shown in Fig. 1(a). The system incorporates three working fluids: intermediate working fluid, air, and fuel. Key components consist of a circulating pump, intermediate working fluid storage tank, valves, flow meter, and two serially arranged HEXs. All components are hydraulically connected in series via the intermediate working fluid loop. Fig. 1(b) illustrates the operating principle of the basic ICHE system. Air serves as the heat source, and fuel acts as the cold-side medium. The intermediate working fluid absorbs heat in HEX-1 and releases it in HEX-2, thereby enabling the indirect transfer of thermal energy from air to fuel.

The ICHE system design primarily centers on the optimization of its integrated HEXs. The intermediate working fluid's circulation temperature and mass flow rate directly influence the overall heat transfer coefficient and the mean temperature difference across the HEXs, thereby affecting both the heat transfer capacity and the required heat transfer area. Given the interconnection of HEXs through the intermediate working fluid, the ICHE system design optimization ultimately depends on identifying the intermediate fluid's optimal thermodynamic parameters, specifically its circulation temperature and mass flow rate, to achieve coordinated optimization of system heat transfer area and thermal performance.

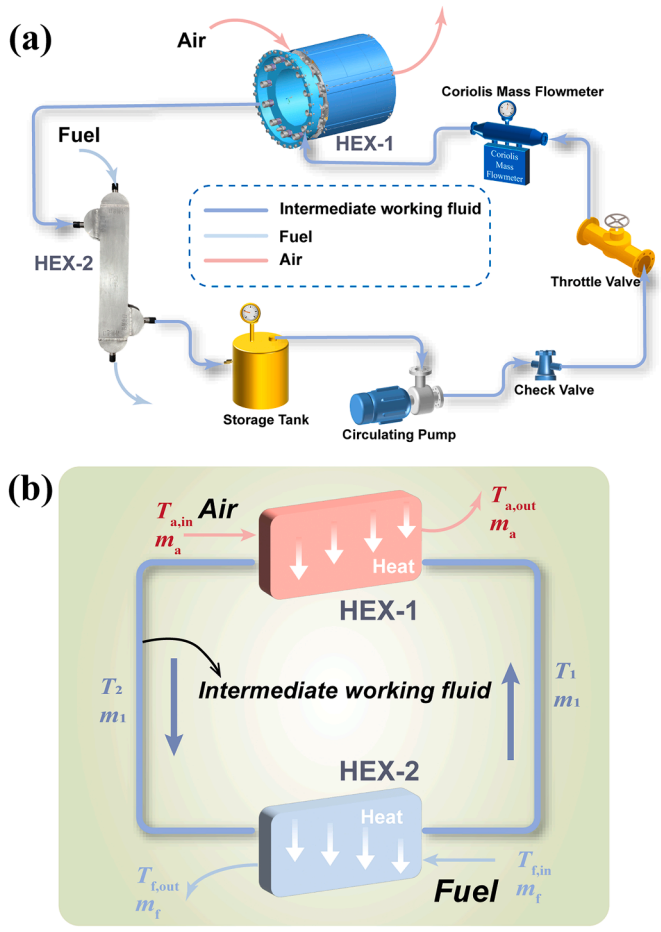

Fig. 1. Schematic diagram of the basic ICHE system for aero engines. (a) Schematic configuration diagram; (b) System principle diagram.

2.2. Multi-branch ICHE system

Fig. 2(a) illustrates the operating principle of the multi-branch ICHE system. Compared with the basic configuration, the multi-branch ICHE system adds parallel branches with at least three HEXs to meet the more complex thermal management demands of aero engines. In the configuration shown in Fig. 2(a), heat sources include compressor bleed air and bearing cavity cooling air, while fuel functions as the sole cooling medium. HEX-1 and HEX-2 are arranged in parallel and coupled via the intermediate working fluid. The intermediate fluid absorbs heat in HEX-1 and HEX-2, mixes downstream, and subsequently releases heat in HEX-3, thereby enabling indirect thermal energy transfer to the fuel.

Unlike the basic ICHE system, the multi-branch ICHE system requires operational optimization of heat transfer rate (Q) distribution. Under steady-state conditions and negligible heat loss, the first law of thermodynamics implies equal Q across the two HEXs in the basic ICHE system. By contrast, in the multi-branch system, total heat extracted from the heat source equals that absorbed by the cooling medium—i.e., the sum of Q in HEX-1 (Q_1) and HEX-2 (Q_2) equals that in HEX-3 (Q_3), which represents the system's heat load. Hence, regulating the heat distribution between Q_1 and Q_2 to maximize Q_3 constitutes the core operational optimization objective for the multi-branch ICHE system. Given the practical operating conditions of aero engines, the key control variables in the operational optimization of a multi-branch ICHE system are the main-loop intermediate working fluid mass flow rate and its distribution ratio among the parallel branches. These parameters directly govern the thermal performance of each HEX within the system and consequently regulate the overall system heat transfer rate.

2.3. Experimental system

To provide experimental data support for the operational optimization of the ICHE system and ensure its reliability, a multi-branch ICHE system experimental platform for aero engines was constructed, as shown in Fig. 2(b). The experimental system involves three working fluids: air, Chinese aviation kerosene RP-3, and high-pressure water.

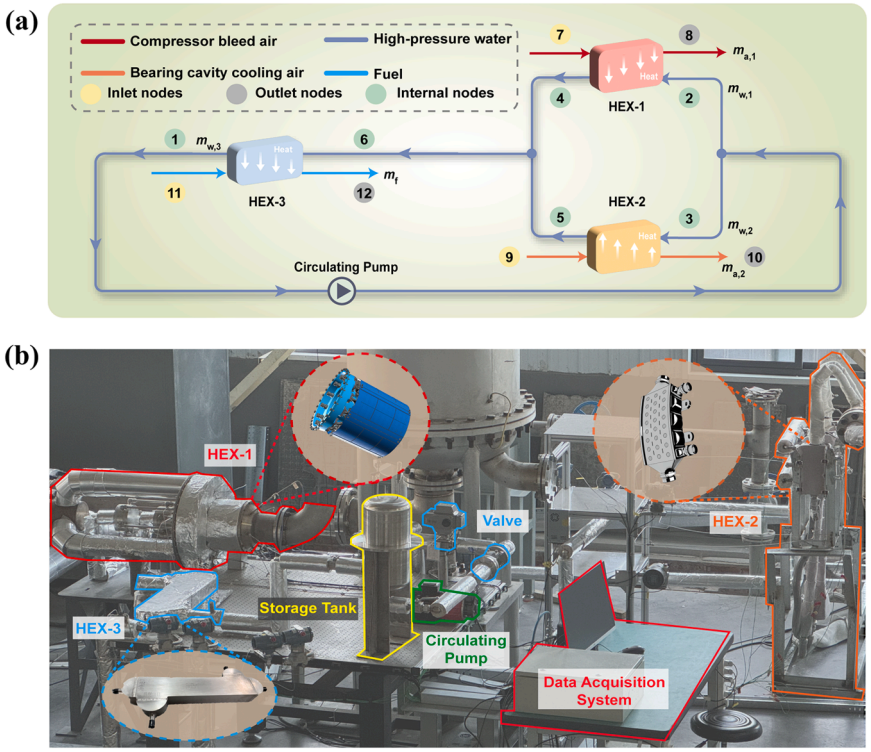

Fig. 2. Schematic diagram of the multi-branch ICHE system for aero engines. (a) Schematic configuration diagram; (b) Experimental setup.

Table 1
The uncertainties of the test rig [15].

Parameters	Uncertainty	Parameters	Uncertainty
Fuel mass flow rate	±0.2%	Air mass flow rate	±0.5%
Water mass flow rate	±0.15%	Temperature	±1.5 K
$Q_{w,1}$	6.24%	$Q_{a,1}$	3.49%
$Q_{w,2}$	4.97%	$Q_{a,2}$	2.36%
Q_f	9.24%	$Q_{w,3}$	4.56%
Q_1	3.58%	Q_2	2.82%
Q_3	5.11%		

High-temperature air is used to simulate compressor bleed air and bearing cavity cooling air, while high-pressure water serves as the intermediate working fluid. It should be noted that using water as an intermediate working fluid is not the sole option. Although water was selected due to its safety, availability, and stability in the experimental system, the proposed optimization framework is general and can be extended to other working fluids. Supercritical CO_2 combines high heat capacity and strong heat transfer capability but requires high-pressure equipment. Helium is chemically inert but has low specific heat, leading to increased pumping demand. Liquid metals such as NaK alloys offer very high thermal conductivity but face safety and material compatibility issues. Considering these trade-offs will be an important direction of future work. The system consists of three functionally distinct HEXs: HEX-1, a serpentine-tube exchanger transferring compressor bleed air heat to water [44]; HEX-2, a shell-and-tube exchanger transferring bearing cavity cooling air heat to water; and HEX-3, a water-to-fuel printed circuit heat exchanger (PCHE) featuring airfoil fins [45]. The uncertainties of directly measured quantities and the maximum uncertainties of indirectly measured quantities in the experimental system are listed in Table 1 [15]. The subscripts 'a', 'f', and 'w' denote air, aviation kerosene, and water, respectively, while '1′, '2′, and '3′ correspond to HEX-1, HEX-2, and HEX-3.

A series of experimental investigations were conducted to examine the thermodynamic characteristics of the multi-branch ICHE system under various parameter conditions, resulting in a comprehensive dataset. Detailed methodologies and the complete dataset are available in our previous study [15]. Throughout the experiments, the relative deviation in heat transfer rate between the hot and cold sides of each HEX remained below 10%, validating the data reliability. Moreover, the relative deviation between Q_3 and (Q_1+Q_2) was less than 8%, indicating minimal heat loss and stable system operation during data acquisition.

3. Mathematical model

A comprehensive optimization framework was established for the ICHE system, addressing both design and operation stages by formulating the energy transport process as a mathematical problem. First, a heat transfer model for HEX was developed to serve as the foundation for system-level design and analysis. Subsequently, for the basic ICHE system, a coordinated optimization model was formulated using total heat transfer area and system-equivalent thermal conductance as dual objectives, and the corresponding Pareto optimality conditions were derived. Finally, for the multi-branch ICHE system, a transfer matrix-based model was applied to perform optimization analysis. The mathematical optimization problems were solved using a hybrid algorithm integrating the GA with the interior-point method.

3.1. Heat transfer model for HEX

In thermal system design, the overall heat transfer coefficient K directly influences the required heat transfer area A of the HEX. Moreover, accurate identification of K is a critical element in the analysis and optimization of system operation.

Using a shell-and-tube HEX as an example, other configurations differ only in the formulation of the solid wall thermal resistance R_{wall} and the heat transfer area ratio between the hot and cold sides. However, the mathematical structure of the overall heat transfer coefficient K remains unchanged and is thus not further elaborated. Assuming the intermediate working fluid flows on the inner side of the HEX, K referenced to the inner surface area is given by:

$$K = \frac{1}{\frac{1}{h_i} + R_{wall} + \frac{1}{h_o}\frac{d_i}{d_o}} \tag{1}$$

where h represents the heat transfer coefficient, R_{wall} is the thermal resistance attributed to thermal conduction across the wall, d is the hydraulic diameter, and subscripts 'i' for the inner side, 'o' for the outer side.

For the intermediate fluid side, the Nusselt number (Nu) correlation is expressed in the Dittus-Boelter form as follows:

$$Nu = CRe_w^a Pr_w^b = \frac{h_i d_i}{\lambda_w} \tag{2}$$

where a, b, and C are the coefficients in the Nu correlation, subscript 'w' represents the intermediate working fluid, and λ, Pr, and Re represent the thermal conductivity, Prandtl number, and Reynolds number of the intermediate fluid, respectively. For internal pipe flow, the values of the coefficients a, b, and C are determined by the flow regime of the intermediate fluid. In the laminar regime, $Nu = 3.66$, whereas in the turbulent regime, the coefficients correspond to those in the Dittus-Boelter correlation [46], as specified in Eq. (3). Moreover, the relationship between Re_w and the intermediate fluid mass flow rate m_w is given by:

$$\begin{cases} (\text{Laminar}) a = 0, b = 0, C = 3.66 \\ (\text{Turbulent}) a = 0.8, b = 0.4, C = 0.023 \end{cases} \tag{3}$$

$$Re_w = \frac{4m_w}{\mu_w \pi d_i n} \tag{4}$$

where μ_w represents intermediate fluid dynamic viscosity, n is the number of heat exchange units.

For simplification, the following two intermediate parameters are defined:

$$\alpha = \left(\frac{4}{\mu_w \pi n}\right)^a \frac{C\lambda_w Pr_w^b}{d_i^{a+1}} \tag{5}$$

$$\beta = R_{wall} + \frac{1}{h_o}\frac{d_i}{d_o} \tag{6}$$

Since the thermal properties of the intermediate fluid can be iteratively updated during the calculation, α is treated as a constant. Thus, the heat transfer coefficient on the intermediate fluid side, h_i, can be expressed as:

$$h_i = \alpha m_w^a \tag{7}$$

The parameter β is determined by the outer fluid heat transfer coefficient, h_o. As indicated in Eq. (8), and similarly to Eq. (7), h_o is a univariate function of the outer fluid mass flow rate (m_o). In system design scenarios where the outer fluid flow rate is fixed, h_o can be treated as constant, and consequently, β is also considered constant. By contrast, in operational optimization, where HEX geometry is predefined, h_o is calculated using appropriate Nu correlations according to the boundary conditions of the outer fluid.

$$h_o = f(m_o) \tag{8}$$

By combining Eqs. (1), (6), and (7), the mathematical model for calculating K is obtained as:

$$K = \frac{\alpha m_w^a}{1 + \alpha\beta m_w^a} \tag{9}$$

Eq. (9) expresses the overall heat transfer coefficient as a function of

the intermediate fluid mass flow rate. This formulation enables the derivation of a simplified objective function for ICHE system design optimization. Furthermore, in the operational optimization of multi-branch ICHE system, it allows for rapid calculation of thermal resistance, thereby supporting the application of the transfer matrix-based method in system analysis and optimization.

3.2. Model for design optimization

In the basic ICHE system model illustrated in Fig. 1(b) (with parameter definitions also given in Fig. 1(b)), only a configuration with two HEXs arranged in series is considered. For more complex, multi-branch ICHE configurations, the objective function forms derived below can be adapted to construct corresponding objective functions tailored to specific system design requirements, thereby enabling system-level design optimization. The objective of ICHE system design optimization is to balance system weight and heat transfer capacity, using the intermediate fluid circulation mass flow rate (m_1) and intermediate temperature (T_1) as control variables. To reflect the model's essential features, the basic ICHE system is simplified under the following assumptions:

(1) Heat losses in pipelines and components during fluid flow are neglected.
(2) The system is in steady-state, with known air and fuel side boundary conditions.
(3) Thermal properties of working fluids remain constant during heat exchange.
(4) Both HEX-1 and HEX-2 are tube-bundle types with counterflow configuration, with the intermediate fluid flowing inside the tubes; tube diameter and unit count are predefined.
(5) For weight optimization, only the mass of the HEXs is considered, while the weight of piping, valves, and auxiliary components is neglected.

Based on the energy conservation equation, the heat transfer rates of the two HEXs within the system can be expressed as follows:

$$Q_1 = m_a c_{p,a}\left(T_{a,in} - T_{a,out}\right) = m_1 c_{p,w}(T_2 - T_1) \tag{10}$$

$$Q_1 = K_1 A_1 \Delta T_{m,1} \tag{11}$$

$$Q_2 = m_f c_{p,f}\left(T_{f,out} - T_{f,in}\right) = m_1 c_{p,w}(T_2 - T_1) \tag{12}$$

$$Q_2 = K_2 A_2 \Delta T_{m,2} \tag{13}$$

where subscripts '1′, '2′, 'a', 'f', 'in', and 'out' respectively represent HEX-1, HEX-2, air, fuel, inlet, and outlet; c_p is the isobaric specific heat capacity; ΔT_m is the mean temperature difference.

When the intermediate cycle heat exchange system is in steady-state operation, the following condition holds:

$$Q_{equal} = Q_1 = Q_2 \tag{14}$$

where Q_{equal} is the system steady-state heat transfer rate.

By combining Eqs. (10-14), the intermediate temperature, heat transfer area, and thermal conductance of each HEX can be expressed as follows:

$$T_2 = \frac{G_a}{G_w}\left(T_{a,in} - T_{a,out}\right) + T_1 = \frac{G_f}{G_w}\left(T_{f,out} - T_{f,in}\right) + T_1 \tag{15}$$

$$A_1 = \frac{Q_{equal}}{K_1 \Delta T_{m,1}} \tag{16}$$

$$A_2 = \frac{Q_{equal}}{K_2 \Delta T_{m,2}} \tag{17}$$

$$(KA)_1 = K_1 A_1 = \frac{Q_{equal}}{\Delta T_{m,1}} \tag{18}$$

$$(KA)_2 = K_2 A_2 = \frac{Q_{equal}}{\Delta T_{m,2}} \tag{19}$$

where G denotes the heat capacity flow rate, defined as the product of mass flow rate m and isobaric specific heat capacity c_p, and (KA) represents the thermal conductance of the HEX.

By combining Eqs. (16) and (17), the expression for the total heat transfer area A_{total} of all HEXs in the system can be derived, where A_{total} is a function of m_1 and T_1:

$$A_{total}(m_1, T_1) = A_1 + A_2 = Q_{equal}\left(\frac{1}{K_1 \Delta T_{m,1}} + \frac{1}{K_2 \Delta T_{m,2}}\right) \tag{20}$$

Considering that A_{total} denotes the total inner-surface heat transfer area of all HEXs in the system, the weight of the heat exchange units can be calculated based on tube wall thickness and material density. Neglecting the weight of auxiliary components such as pipelines and valves within the ICHE system, A_{total} is thus used to represent the system weight. Consequently, minimizing system weight becomes equivalent to minimizing A_{total}.

The thermal conductance KA of a HEX quantifies the heat transfer rate per unit temperature difference, thus reflecting its intrinsic heat transfer potential under a given temperature difference. For a single HEX, an increase in KA corresponds to reduced thermal resistance and an enhanced driving force for heat exchange. Within an ICHE system, the system-equivalent thermal conductance $(KA)_{sys}$ characterizes the intermediate loop's overall capacity to transfer heat from air to fuel. A greater $(KA)_{sys}$ value indicates higher heat transfer capability under identical temperature differences, suggesting improved overall system heat transfer performance. Thus, optimizing system heat transfer capacity becomes equivalent to maximizing $(KA)_{sys}$.

For the basic ICHE system depicted in Fig. 1(b), where two HEXs are connected in series and the same heat flow Q_{equal} sequentially passes through HEX-1 and HEX-2, the thermal resistances of the series configuration are additive. Since KA is the reciprocal of thermal resistance, the system-equivalent total thermal conductance $(KA)_{sys}$ is calculated as follows, where $(KA)_{sys}$ is a function of m_1 and T_1:

$$(KA)_{sys} = \frac{1}{\frac{1}{(KA)_1} + \frac{1}{(KA)_2}} = \frac{Q_{equal}}{\Delta T_{m,1} + \Delta T_{m,2}} \tag{21}$$

As indicated by Eqs. (20) and (21), the ICHE system's design optimization depends on calculating the mean temperature difference ΔT_m across the HEXs. In HEX design, the logarithmic mean temperature difference (LMTD) is commonly employed [47]. However, when the heat capacity flow rates of hot and cold fluids are equal, LMTD becomes inapplicable. In these situations, the arithmetic mean temperature difference (AMTD) provides a more suitable alternative. It can be demonstrated that when $\Delta T_{max} / \Delta T_{min} < 1.2$ (where ΔT_{max} and ΔT_{min} represent the larger and smaller values among the inlet and outlet temperature differences, respectively), the relative error between LMTD and AMTD remains below 0.28% [25]. Therefore, to ensure computational continuity and consistency, the mean temperature difference is evaluated using the following expression:

$$\begin{cases} \dfrac{\max\{(T_{a,in}-T_2),(T_{a,out}-T_1)\}}{\min\{(T_{a,in}-T_2),(T_{a,out}-T_1)\}} \le 1.2, \Delta T_{m,1} = \dfrac{T_{a,in}-T_2+T_{a,out}-T_1}{2} \\ \dfrac{\max\{(T_2-T_{f,out}),(T_{a,out}-T_1)\}}{\min\{(T_2-T_{f,out}),(T_{a,out}-T_1)\}} \le 1.2, \Delta T_{m,2} = \dfrac{T_2-T_{f,out}+T_1-T_{f,in}}{2} \\ \dfrac{\max\{(T_{a,in}-T_2),(T_{a,out}-T_1)\}}{\min\{(T_{a,in}-T_2),(T_{a,out}-T_1)\}} > 1.2, \Delta T_{m,1} = \dfrac{(T_{a,in}-T_2)-(T_{a,out}-T_1)}{\ln[(T_{a,in}-T_2)/(T_{a,out}-T_1)]} \\ \dfrac{\max\{(T_2-T_{f,out}),(T_{a,out}-T_1)\}}{\min\{(T_2-T_{f,out}),(T_{a,out}-T_1)\}} > 1.2, \Delta T_{m,2} = \dfrac{(T_2-T_{f,out})-(T_1-T_{f,in})}{\ln[(T_2-T_{f,out})/(T_1-T_{f,in})]} \end{cases} \tag{22}$$

Building upon the above analysis, the ICHE system's design optimization involves two inherently conflicting objectives: A_{total} and $(KA)_{sys}$. These two objectives represent opposing physical tendencies, necessitating a trade-off to achieve a balanced, integrated optimum. To enable coordinated optimization tailored to specific design needs, this study applies a normalization process and incorporates a weighting factor ω to linearly combine the two objectives into a scalar function. This reformulates the multi-objective optimization problem into a conventional single-objective form, as expressed by the following equation:

$$F(m_1, T_1) = \omega \frac{A_{total}(m_1, T_1)}{A_0} + (1-\omega)\frac{-(KA)_{sys}(m_1, T_1)}{(KA)_0} \tag{23}$$

In this expression, F represents the composite optimization objective, which is to be minimized. The parameter $\omega \in [0, 1]$ is the weighting factor, while A_0 and $(KA)_0$ are the nominal values used for non-dimensionalization. The function A_{total} is defined in Eq. (20), and the function $(KA)_{sys}$ is defined in Eq. (21).

Fundamentally, this method assesses the performance of ICHE system design schemes across varying thermodynamic parameters of the intermediate fluid through the introduction of a composite metric F. The weighting factor ω simultaneously serves as a practical design indicator under realistic engineering conditions. Adjusting ω enables the generation of diverse trade-off solutions within a unified optimization framework. At $\omega = 1$, the objective simplifies to minimizing A_{total}, thereby transforming the original multi-objective problem into one focused solely on reducing system weight. Conversely, at $\omega = 0$, only $-(KA)_{sys}$ is considered, and the problem becomes one of maximizing system-equivalent thermal conductance. For intermediate values $0 < \omega < 1$, the objective reflects varying trade-off intensities: a larger ω emphasizes system weight minimization, while a smaller value prioritizes heat transfer performance. Solving the model across a range of ω values yields the Pareto front of the ICHE system design optimization.

For Eq. (23), by neglecting boundary constraints and applying classical optimization theory to seek extrema, the points satisfying $\nabla F = 0$ are identified as the candidate optimal solution set. This can be formally written as:

$$\begin{cases} \dfrac{\partial F}{\partial T_1} = \dfrac{\omega}{A_0}\dfrac{\partial A_{total}}{\partial T_1} - \dfrac{1-\omega}{(KA)_0}\dfrac{\partial (KA)_{sys}}{\partial T_1} = 0 \\ \dfrac{\partial F}{\partial m_1} = \dfrac{\omega}{A_0}\dfrac{\partial A_{total}}{\partial m_1} - \dfrac{1-\omega}{(KA)_0}\dfrac{\partial (KA)_{sys}}{\partial m_1} = 0 \end{cases} \tag{24}$$

The necessary condition for the optimal solution is derived by transforming Eq. (24), expressed as Eq. (25). Besides, it indicates that the optimal solution satisfies the gradient collinearity condition, where each value of ω corresponds to a specific Pareto optimal point. By assigning different values of ω and solving the equation, various points along the Pareto front can be obtained.

$$\frac{\partial A_{total}/\partial T_1}{\partial (KA)_{sys}/\partial T_1} = \frac{\partial A_{total}/\partial m_1}{\partial (KA)_{sys}/\partial m_1} = \frac{A_0(1-\omega)}{(KA)_0 \omega} \tag{25}$$

The optimization process must adhere to constraints imposed by the ICHE system's characteristics. First, the feasible ranges of m_1 and T_1 must be defined based on engine design and operation conditions. This constraint limits parameter selection and ensures the practical applicability of the optimization results. Second, for a liquid-phase intermediate working fluid, it must remain in a subcooled state throughout operation, i.e., its temperature must not exceed the boiling point T_{limit}. Boiling disrupts flow uniformity and stability, compromising the steady-state operation of the ICHE system. Finally, the system must comply with the second law of thermodynamics. Specifically, at each HEX's inlet and outlet, the cold-side fluid temperature must remain below that of the hot side. Considering these factors, the constraints governing ICHE system design optimization can be formulated as follows:

$$\begin{cases} T_{a,in} - T_2 > 0 \\ T_{a,out} - T_1 > 0 \\ T_2 - T_{f,out} > 0 \\ T_1 - T_{f,in} > 0 \\ T_{limit} - T_2 > 0 \end{cases} \tag{26}$$

Given the nonlinear, multi-constrained, and non-convex characteristics of the ICHE system design optimization problem, this work developed a MATLAB R2021b-based hybrid optimization framework integrating the GA and gradient-based interior-point method [48]. The GA component performs a coarse global search to identify a set of promising initial solutions. These solutions are subsequently refined using the interior-point method, overcoming GA's limitations while exploiting the method's strength in handling nonlinear constraints. Throughout the solution process, the weighting factor ω is varied from 0 to 1, enabling repeated single-objective optimizations to obtain trade-off solutions. This procedure facilitates the construction of the Pareto front. The detailed algorithmic flow is presented in Fig. 3.

The aforementioned method generates a set of optimized solutions by varying ω from 0 to 1. However, the discrete selection of ω values in practical computations may yield a sparse Pareto set, potentially limiting representation of the full Pareto front. To address this limitation, a parallel multi-objective optimization approach based on the Non-dominated Sorting Genetic Algorithm II (NSGA-II) is also employed. The Pareto fronts obtained from both methods are compared to ensure the accuracy and completeness of the ICHE system design optimization results. As NSGA-II is a well-established method [49], its procedural details are omitted for brevity.

3.3. Model for operational optimization

For the model illustrated in Fig. 2(a) (with parameter definitions also given in Fig. 2(a)), the operational optimization of the multi-branch ICHE system aims to maximize the total system heat transfer rate. The control variables are the main-loop intermediate working fluid mass flow rate ($m_{w,3}$) and the flow distribution ratio (ζ). ζ is defined as the ratio of the intermediate working fluid mass flow rate in HEX-1 ($m_{w,1}$) to the main loop intermediate working fluid mass flow rate ($m_{w,3}$), as shown in Eq. (27). This allows the ICHE system to fully utilize the diverse energy streams within the aero engine across the entire flight envelope. To reflect the model's essential features, the multi-branch ICHE system is simplified under the following assumptions:

(1) Heat losses in pipelines and components during fluid flow are neglected.
(2) The system is in steady-state, with known air and fuel side inlet boundary conditions. The system operates under steady-state conditions, with known mass flow rates, inlet temperatures, and inlet pressures of the compressor bleed air, bearing cavity cooling air, and fuel.
(3) Thermal properties of working fluids remain constant during heat exchange.

$$\zeta = m_{w,1}/m_{w,3} \tag{27}$$

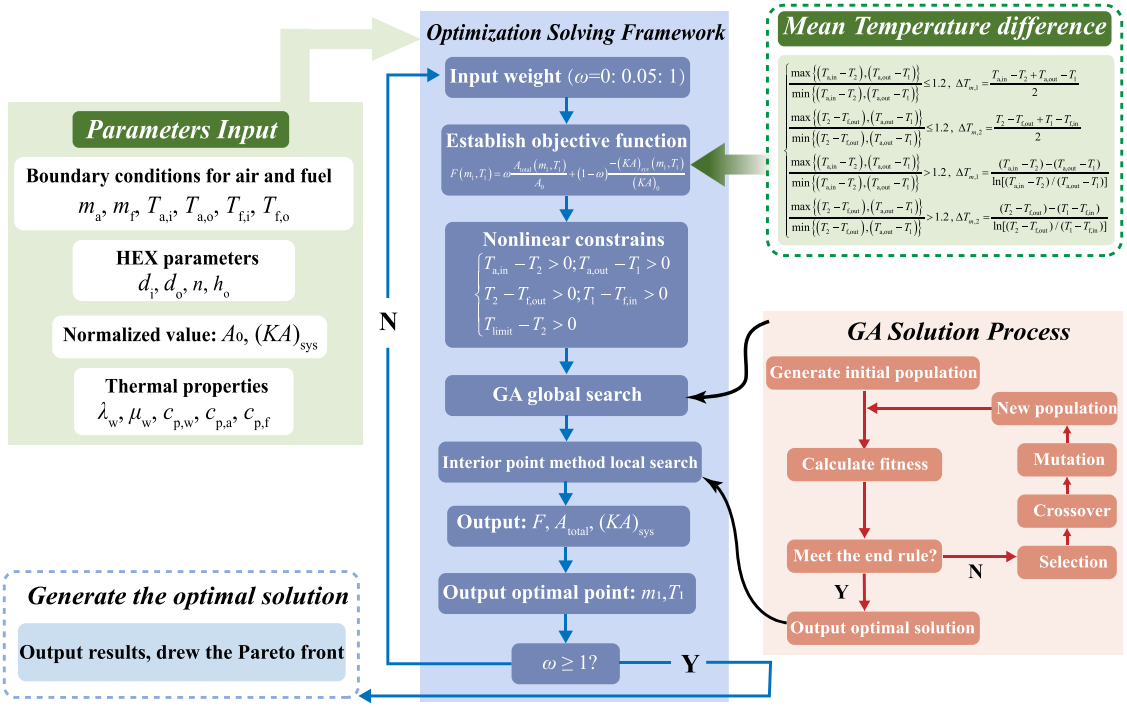

Fig. 3. The flowchart of the ICHE system design optimization.

Accurately identifying the system's thermodynamic performance across different operating parameters is essential for optimizing the multi-branch ICHE system, as it enables the search for optimal control strategies. To achieve this, the study employs the transfer matrix-based modeling method [50,51], grounded in the heat transfer model for HEX, to calculate the system's thermodynamic parameters. This modeling approach constructs a global energy flow topology that captures both component behavior and network constraints, facilitating efficient and robust system-level computations.

The previous work [15] developed a transfer matrix-based model for the multi-branch ICHE system depicted in Fig. 2 and analyzed the effects of various parameters on system thermodynamics. Building on this foundation, the current study integrates the heat transfer model for HEX from Section 3.1 with the transfer matrix-based modeling method, extending its applicability to operational optimization of thermal systems. To maintain brevity, the core steps of the calculation and modeling procedures is presented.

For the multi-branch ICHE system shown in Fig. 2, nodes are categorized into inlet nodes, outlet nodes, and internal nodes based on their physical characteristics. The temperature vectors corresponding to each type of node are expressed as follows:

$$\begin{cases} \mathbf{T}_{\text{in}} = [T_7 T_9 T_{11}]^\top \\ \mathbf{T}_{\text{out}} = [T_8 T_{10} T_{12}]^\top \\ \mathbf{T}_{\text{internal}} = [T_1 T_2 T_3 T_4 T_5 T_6]^\top \\ \mathbf{T} = [T_1 T_2 T_3 T_4 T_5 T_6 T_7 T_8 T_9 T_{10} T_{11} T_{12}]^\top \end{cases} \tag{28}$$

The thermal resistance of HEX based on the inlet temperature difference can be defined as [41]:

$$R = \frac{G_c \exp\left(\frac{KA}{G_h}\right) - G_h \exp\left(\frac{KA}{G_c}\right)}{G_h G_c \left[\exp\left(\frac{KA}{G_h}\right) - \exp\left(\frac{KA}{G_c}\right)\right]} \tag{29}$$

where subscript 'c' and 'h' respectively represent the cold-side fluid and hot-side fluid. The overall heat transfer coefficient K is calculated by the heat transfer model detailed in Section 3.1.

The transfer matrix formulation of the system is given as follows:

$$\mathbf{H}_l \mathbf{T} = \mathbf{H}_r \mathbf{T} \tag{30}$$

where $\boldsymbol{H}_l$ and $\boldsymbol{H}_r$ are coefficient matrices, expressed as:

$$\mathbf{H}_l = \begin{pmatrix} 1&0&0&0&0&0&0&0&0&0&0&0 \\ 0&1&0&0&0&0&0&0&0&0&0&0 \\ 0&0&1&0&0&0&0&0&0&0&0&0 \\ 0&0&0&1&0&0&0&0&0&0&0&0 \\ 0&0&0&0&1&0&0&0&0&0&0&0 \\ 0&0&0&0&0&1&0&0&0&0&0&0 \\ 0&0&0&0&0&0&0&0&0&0&0&0 \\ 0&0&0&0&0&0&0&1&0&0&0&0 \\ 0&0&0&0&0&0&0&0&0&0&0&0 \\ 0&0&0&0&0&0&0&0&0&1&0&0 \\ 0&0&0&0&0&0&0&0&0&0&0&0 \\ 0&0&0&0&0&0&0&0&0&0&0&1 \end{pmatrix} \tag{31}$$

$$\mathbf{H}_r = \begin{pmatrix} 0&0&0&0&0&1-s_3&0&0&0&0&s_3&0 \\ 1&0&0&0&0&0&0&0&0&0&0&0 \\ 1&0&0&0&0&0&0&0&0&0&0&0 \\ 0&1-t_1&0&0&0&0&t_1&0&0&0&0&0 \\ 0&0&1-t_2&0&0&0&0&0&t_2&0&0&0 \\ 0&0&0&f&1-f&0&0&0&0&0&0&0 \\ 0&0&0&0&0&0&0&0&0&0&0&0 \\ 0&s_1&0&0&0&0&1-s_1&0&0&0&0&0 \\ 0&0&0&0&0&0&0&0&0&0&0&0 \\ 0&0&s_2&0&0&0&0&0&1-s_2&0&0&0 \\ 0&0&0&0&0&0&0&0&0&0&0&0 \\ 0&0&0&0&0&t_3&0&0&0&0&1-t_3&0 \end{pmatrix} \tag{32}$$

where let $f = (mc_p)_4/[(mc_p)_4+(mc_p)_5]$, and the calculation coefficients s_i and t_i are defined as below:

$$\begin{cases} s_i = \dfrac{1}{(RG_h)_i} \\ t_i = \dfrac{1}{(RG_c)_i} \end{cases}, i = 1,2,3 \tag{33}$$

In Eq. (33), subscripts '1′, '2′, and '3′ respectively denote HEX-1, HEX-2, and HEX-3. By eliminating the redundant rows and columns

from Eq. (30), a simplified form of the transfer matrix equation is derived as follows:

$$\begin{pmatrix} T_1 \\ T_2 \\ T_3 \\ T_4 \\ T_5 \\ T_6 \\ T_8 \\ T_{10} \\ T_{12} \end{pmatrix} = \begin{pmatrix} 0 & 0 & 0 & 0 & 0 & 1-s_3 & 0 & 0 & s_3 \\ 1 & 0 & 0 & 0 & 0 & 0 & 0 & 0 & 0 \\ 1 & 0 & 0 & 0 & 0 & 0 & 0 & 0 & 0 \\ 0 & 1-t_1 & 0 & 0 & 0 & 0 & t_1 & 0 & 0 \\ 0 & 0 & 1-t_2 & 0 & 0 & 0 & 0 & t_2 & 0 \\ 0 & 0 & 0 & f & 1-f & 0 & 0 & 0 & 0 \\ 0 & s_1 & 0 & 0 & 0 & 0 & 1-s_1 & 0 & 0 \\ 0 & 0 & s_2 & 0 & 0 & 0 & 0 & 1-s_2 & 0 \\ 0 & 0 & 0 & 0 & 0 & t_3 & 0 & 0 & 1-t_3 \end{pmatrix} \begin{pmatrix} T_1 \\ T_2 \\ T_3 \\ T_4 \\ T_5 \\ T_6 \\ T_7 \\ T_9 \\ T_{11} \end{pmatrix} \tag{34}$$

Reformulating the Eq. (34) on the basis of the outlet and internal nodes, the following expression can be obtained:

$$\begin{pmatrix} \mathbf{T}_{\text{internal}} \\ \mathbf{T}_{\text{out}} \end{pmatrix} = \begin{pmatrix} \mathbf{H}_{m,r}^{1,1} & \mathbf{H}_{m,r}^{1,2} \\ \mathbf{H}_{m,r}^{2,1} & \mathbf{H}_{m,r}^{2,2} \end{pmatrix} \begin{pmatrix} \mathbf{T}_{\text{internal}} \\ \mathbf{T}_{\text{in}} \end{pmatrix} \tag{35}$$

Here, $\boldsymbol{H}_{m,r}$ is the reduced version of $\boldsymbol{H}_r$, and the dimensions of blocks $\mathbf{H}_{m,r}^{ij}$ same with those of $\boldsymbol{T}_{\text{in}}$, $\boldsymbol{T}_{\text{out}}$, and $\boldsymbol{T}_{\text{internal}}$.

Further, by applying block matrix multiplication to decompose Eq. (35) into two separate equations and rearranging the terms, the thermodynamic equations of the multi-branch ICHE system can be obtained as below:

$$\begin{cases} \left(\mathbf{I} - \mathbf{H}_{m,r}^{1,1}\right)\mathbf{T}_{\text{internal}} = \mathbf{H}_{m,r}^{1,2}\mathbf{T}_{\text{in}} \\ \mathbf{T}_{\text{out}} = \mathbf{H}_{m,r}^{2,1}\mathbf{T}_{\text{internal}} + \mathbf{H}_{m,r}^{2,2}\mathbf{T}_{\text{in}} \end{cases} \tag{36}$$

By inputting $\boldsymbol{T}_{\text{in}}$ and the mass flow rates of each working fluid within the system, and incorporating the heat transfer model for HEXs, the temperatures at all nodes in the system can be calculated using Eq. (36). To account for the temperature-dependent thermal properties, a fixed-point iteration is employed. The process begins with an initial assumption of the fluid properties, followed by the calculation of temperature profiles. The properties are then updated based on the newly obtained temperatures, and the procedure is repeated until convergence is achieved. The thermophysical properties of air and water are obtained from the open-source database CoolProp [52], while those of aviation kerosene RP-3 are sourced from the literature [11,53–55].

Based on the above transfer matrix-based model, the objective function for the operational optimization of the multi-branch ICHE system is calculated as follows:

$$Q_3 = m_{\text{f}} c_{\text{p,f}} (T_{12} - T_{11}) = m_{\text{w,3}} c_{\text{p,w3}} (T_6 - T_1) \tag{37}$$

The operational optimization of the multi-branch ICHE system adheres to constraints similar to those outlined in Section 3.2 for design optimization. The second law of thermodynamics must be satisfied, which is inherently ensured by the transfer matrix-based model. It is also necessary to maintain the intermediate fluid in a subcooled state, with its temperature consistently below the boiling point T_{limit}. Additionally, under practical aero engine conditions, the fuel temperature must remain below its maximum permissible limit, $T_{\text{fuel,max}}$. This constraint is governed by the fuel's coking onset temperature and the downstream utilization requirements. For instance, thermal oxidative coking of aviation kerosene initiates near 150 °C [56], with substantial deposits forming above 280 °C [57]. Thus, setting $T_{\text{fuel,max}}$ to 250 °C offers a practical compromise between heat sink utilization and long-term operational stability, minimizing the risk of coking-induced blockages. Taking all these factors into consideration, the governing constraints for ICHE system operation optimization are formulated as follows:

$$\begin{cases} T_{\text{fuel,max}} - T_{12} > 0 \\ T_{\text{limit}} - T_4 > 0 \\ T_{\text{limit}} - T_5 > 0 \end{cases} \tag{38}$$

A hybrid solution framework for ICHE system operational optimization is developed based on transfer matrix-based modeling, as shown in Fig. 4. The framework comprises three core modules: a parameter input module, a thermal parameters solving module, and an optimization module. The thermal parameter solving module employs the transfer matrix-based modeling approach to compute the nodal temperatures of the multi-branch ICHE system and updates the reference temperature through fixed-point iteration. The optimization module, similar to that in Section 3.2, integrates the GA with a gradient-based interior-point method to refine solutions efficiently.

4. Optimization results and case analyses

Using the proposed models, both design and operational optimization were conducted on a representative aero engine ICHE system to validate the framework's accuracy and robustness. The ICHE system utilizes aviation kerosene RP-3 as fuel and high-pressure water as the intermediate working fluid.

4.1. Design optimization for basic ICHE system

A coordinated optimization of heat transfer area and thermal performance was performed for the basic ICHE system illustrated in Fig. 1 (b). The operating condition is specified in Table 2. Table 3 lists the fundamental structural parameters of HEXs, assuming the tube-bundle HEX configuration with counterflow arrangement. Based on typical aero engine HEX performance and the studied conditions, the nominal scalarization values for the objective function are set as $A_0 = 1.3983\ \text{m}^2$, $(KA)_0 = 823.08$ W/K. The intermediate fluid's thermodynamic parameter ranges are defined as $m_1 \in [0.1, 3]$kg/s, $T_1 \in [55, T_{\text{limit}}]$°C. Given a water pressure of 4.50 MPa (P_1), the corresponding boiling point is $T_{\text{limit}} = 257.44$ °C.

The hybrid optimization algorithm developed for ICHE system design (Fig. 3) was applied to determine optimal intermediate fluid thermodynamic parameters under varying weighting factors ω, thereby generating the Pareto front. To validate the model's accuracy, an exhaustive calculation of the objective function was performed. Specifically, the parameter ranges of m_1 and T_1 were each discretized into at least 500 segments, resulting in over 250,000 (m_1, T_1) combinations. Eq. (23) was evaluated for each combination to yield the complete distribution of F values. Optimization results from both the algorithm and the exhaustive grid search under various ω values are summarized in Table 4. A maximum relative deviation of just 0.13% was observed, confirming the high accuracy of the proposed algorithm.

Table 4 demonstrates that the maximum deviation occurs at $\omega = 0$, where Eq. (23) reduces to Eq. (39), converting the coordinated optimization into a single-objective problem to maximize $(KA)_{\text{sys}}$. Notably, for exhaustive calculation, achieving accurate optimization of $(KA)_{\text{sys}}$ under this condition requires over 2.25 million grid points, far exceeding the initial 250,000. Even with 49 million grid points, accuracy gains remain marginal, while computational cost becomes prohibitive. The optimization algorithm yields a maximum $(KA)_{\text{sys}}$ of 829.53 W/K, compared to 795.72 W/K from the 250,000-point exhaustive method, with a 4.25% relative deviation. This suggests the 250,000-point resolution was too coarse to capture the optimal (m_1, T_1). Accordingly, this study conducted exhaustive calculations at various grid densities and compared their computational times, as shown in Fig. 5. Initially, the original range of m_1 and T_1 was discretized. Further increasing the number of grid points yielded diminishing returns. At 49 million points, the maximum $(KA)_{\text{sys}}$ obtained was 819.14 W/K, with a relative deviation of 1.27%, while the computation time increased significantly to 129,011 seconds. Based on these results, a refined local grid search was conducted in the narrowed region 2.85 kg/s $< m_1 <$ 3 kg/s, 140 °C $< T_1 <$ 155 °C. At 9 million points, the search produced 828.49 W/K in 5876 seconds, with a relative deviation of only 0.13%, which effectively matched the optimization result.

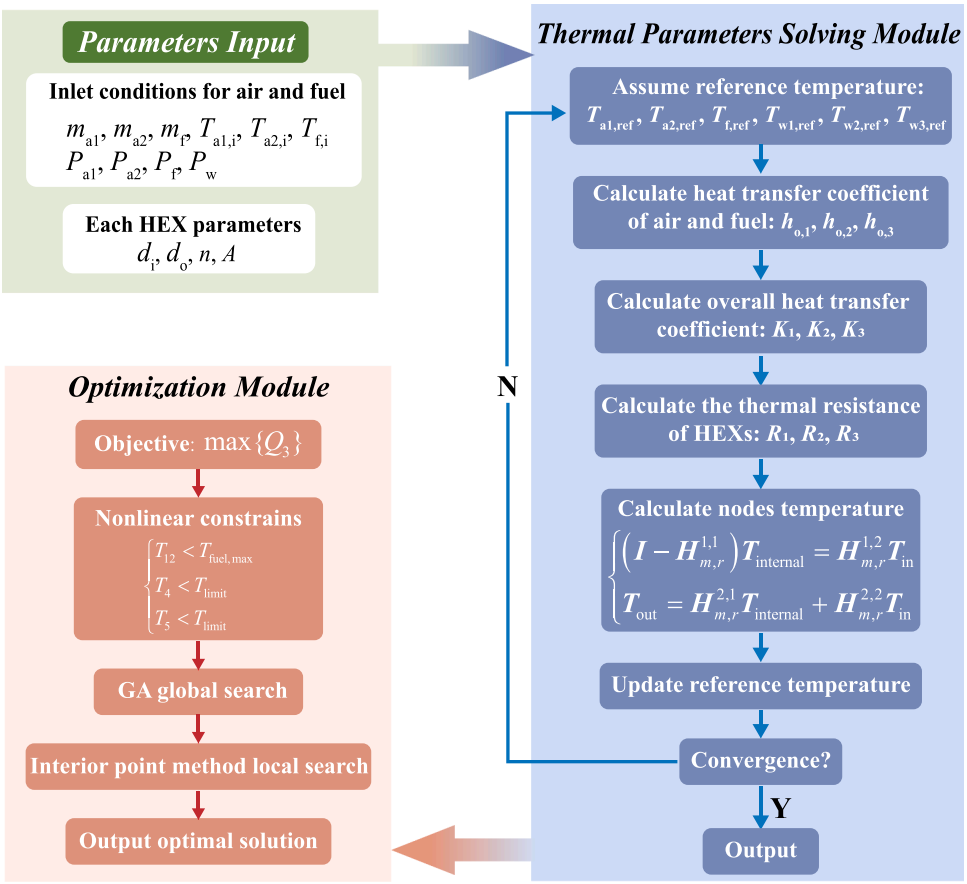

Fig. 4. The flowchart of the ICHE system operational optimization.

Table 2
Operating parameters for design optimization of basic ICHE system.

Parameter	Value	Parameter	Value
m_a (kg/s)	1.28	$T_{a,in}$ (°C)	312
m_f (kg/s)	0.44	$T_{a,out}$ (°C)	236
$c_{p,a}$ (J/(kg·K))	1042.4	$T_{f,in}$ (°C)	54
$c_{p,f}$ (J/(kg·K))	2227.7	$T_{f,out}$ (°C)	157.46
$c_{p,w}$ (J/(kg·K))	4212.4	$P_{a,in}$ (MPa)	0.88
$h_{o,1}$ (W/(m^2·K))	750	$P_{f,in}$ (MPa)	0.53
$h_{o,2}$ (W/(m^2·K))	5000	P_1 (MPa)	4.50
A_0 (m^2)	1.3983	$(KA)_0$ (W/K)	823.08

Table 3
Structure parameters of the HEX in the basic ICHE system.

	HEX-1	HEX-2
n	192	200
λ_{wall} (W/(m·K))	16.2	16.2
d_i (mm)	1.4	1.2
d_o (mm)	1.8	1.6
Material	316L Stainless Steel	316L Stainless Steel

$$F(m_1, T_1) = \frac{-(KA)_{sys}(m_1, T_1)}{(KA)_0} \tag{39}$$

The above findings demonstrate that, for a given ω, conventional grid-based methods show substantial inefficiency in determining design points. They demand excessive time and resources, requiring many grid points to reach a grid-independent solution. Even at 1.52% deviation (requiring 2.25 million points), each calculation takes approximately 1500 seconds. In contrast, the optimization algorithm developed in this study reaches comparable accuracy in under 20 seconds, representing an approximately 75-fold improvement in efficiency. This greatly enhances the computational effectiveness of ICHE system design optimization for aero engines.

Table 4
Comparison between optimization algorithm results and exhaustive calculation results for ICHE system design optimization.

ω	Optimization results			Exhaustive grid search results			Error in F (%)
	F	A_{total} (m^2)	$(KA)_{sys}$ (W/K)	F	A_{total} (m^2)	$(KA)_{sys}$ (W/K)	
0.00	-1.01	4.46	829.53	-1.01	4.38	828.49	0.13
0.05	-0.83	2.79	801.43	-0.83	2.85	803.38	0.01
0.10	-0.69	2.13	771.59	-0.69	2.04	765.25	0.06
0.15	-0.58	1.79	743.53	-0.58	1.77	741.37	0.01
0.20	-0.47	1.59	718.47	-0.47	1.58	717.01	0.00
0.25	-0.37	1.49	702.53	-0.37	1.49	702.77	0.00
0.30	-0.28	1.45	694.19	-0.28	1.45	693.64	0.00
0.35	-0.18	1.44	689.54	-0.18	1.44	689.00	0.00
0.40	-0.09	1.43	686.65	-0.09	1.43	686.99	0.00
0.45	0.00	1.42	684.70	0.00	1.42	684.49	-0.13
0.50	0.09	1.42	683.30	0.09	1.42	683.43	0.00
0.55	0.19	1.42	682.24	0.19	1.42	682.62	0.00
0.60	0.28	1.42	681.42	0.28	1.42	681.09	0.00
0.65	0.37	1.42	680.77	0.37	1.42	681.09	0.00
0.70	0.46	1.42	680.23	0.46	1.42	680.36	0.00
0.75	0.55	1.42	679.78	0.55	1.42	679.66	0.00
0.80	0.65	1.40	650.70	0.65	1.40	650.82	0.00
0.85	0.73	1.40	641.31	0.73	1.40	641.20	0.00
0.90	0.82	1.40	635.74	0.82	1.40	635.83	0.00
0.95	0.91	1.40	631.93	0.91	1.40	632.05	0.00
1.00	1.00	1.40	629.13	1.00	1.40	628.99	0.00

Fig. 6 presents the contour map of the objective function F as a function of m_1 and T_1 at $\omega = 0.8$. Two infeasible regions can be observed,

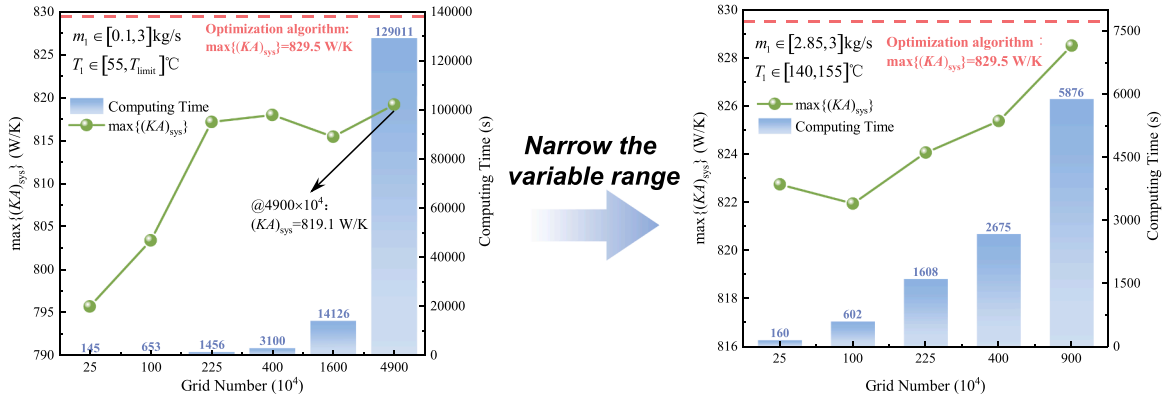

Fig. 5. Comparison of calculation results and time consumption for different exhaustive points.

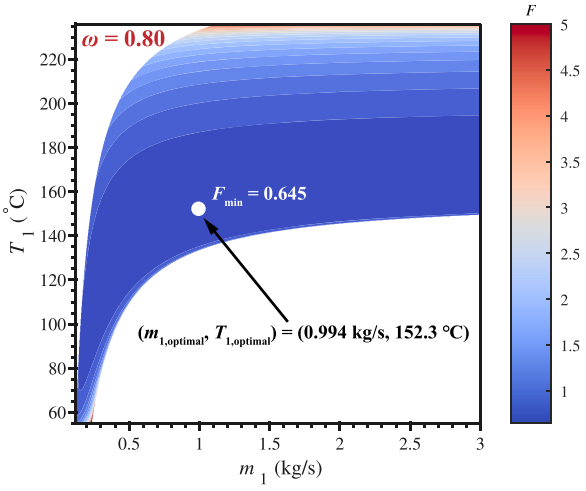

Fig. 6. The distribution of F with respect to m_1 and T_1 at $\omega = 0.8$.

where (m_1, T_1) combinations do not yield valid F values. These occur due to violations of nonlinear constraints, making the results physically or practically infeasible. Additionally, at $\omega = 0.8$, the basic ICHE system exhibits a broad region around the optimal solution, within which multiple (m_1, T_1) combinations yield near-minimal F values. It indicates that for this weighting factor, the selection of intermediate fluid thermodynamic parameters (m_1, T_1) allows for considerable flexibility, enabling near-optimal coordination between A_{total} and $(KA)_{sys}$ across a range of design choices. However, this phenomenon is not consistent across all values of ω. Fig. 7 demonstrates contour maps of the objective function F with respect to m_1 and T_1 for 21 ω values (ranging from 0 to 1 in increments of 0.05); optimal points are marked with black circles. It can be observed that several optimal (m_1, T_1) combinations lie near the boundaries, where slight changes in either m_1 or T_1 may cause significant F variations.

Fig. 8 illustrates the distribution of optimal design parameters—heat transfer area A and thermal conductance KA—obtained from the coordinated optimization of the basic ICHE system under varying ω, using the hybrid optimization algorithm. As ω increases, indicating a greater emphasis on system weight in the objective function, A_2 rapidly decreases and then stabilizes for $\omega > 0.4$. The variation in A_1 is minimal, with a local maximum near $\omega = 0.7$. Consequently, the total heat transfer area A_{total} initially declines rapidly, then plateaus with increasing ω. Thermal conductance KA shows similar behavior: $(KA)_2$ declines rapidly, stabilizing for $\omega > 0.4$, while $(KA)_1$ peaks at $\omega = 0.75$ after a rise and fall. Unlike A_1, $(KA)_1$ is more sensitive to ω, reflecting stronger parameter dependence. As $(KA)_{sys}$ is limited by the smaller HEX thermal conductance, it decreases rapidly, levels off in $0.4 < \omega < 0.75$, and declines again beyond.

The variation trends of A and KA with respect to ω can be explained

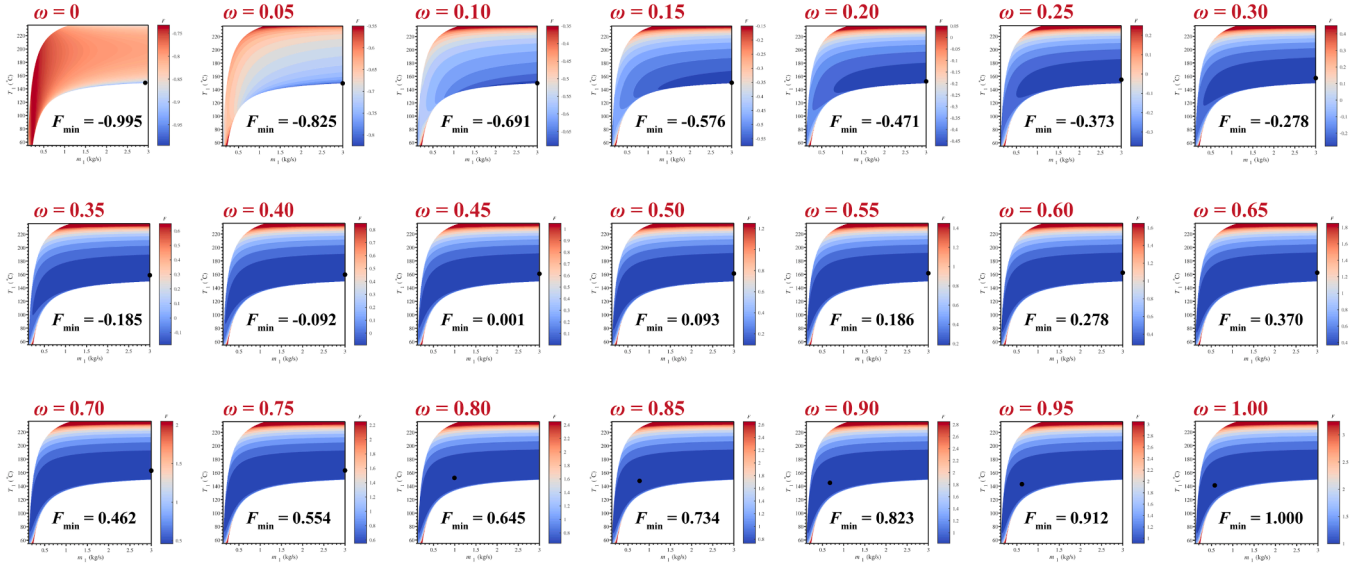

Fig. 7. The distribution of F with respect to m_1 and T_1 under different weighting factors.

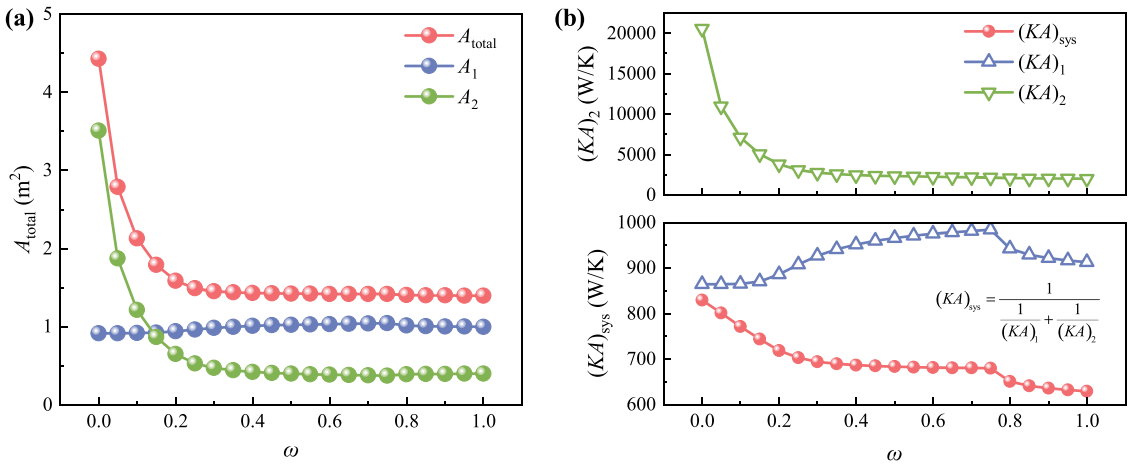

Fig. 8. Effect of weighting factor ω on (a) heat transfer area A; (b) thermal conductance KA.

by the changes in mean temperature differences and intermediate fluid temperatures, as illustrated in Fig. 9. For HEX-2, $\Delta T_{m,2}$ increases monotonically with ω, though at a diminishing rate. Besides, beyond $\omega > 0.4$, the change becomes more gradual. The wide variation of $\Delta T_{m,2}$ explains the more pronounced variations observed in both A_2 and $(KA)_2$. In contrast, for HEX-1, $\Delta T_{m,1}$ decreases before increasing, with a turning point at $\omega = 0.75$. However, the overall fluctuation of $\Delta T_{m,1}$ remains within 16 K, resulting in a limited impact on A_1. Fig. 9(b) further confirms these trends, with inflection points in T_1 and T_2 near $\omega = 0.75$. Moreover, Fig. 9(b) presents that the maximum temperature of the intermediate fluid T_2 remains well below T_{limit} under all ω values, confirming system stability with no boiling.

The Pareto front of the coordinated optimization of system heat transfer area and thermal conductance for the basic ICHE system is shown in Fig. 10. Fig. 10(a) depicts the optimal scalarized objective function F, outlining its lower boundary under different values of ω. Since the nominal values A_0 and $(KA)_0$ were selected to approximately correspond to the values of A_{total} at $\omega = 1$ and $(KA)_{sys}$ at $\omega = 0$, the resulting values of F vary between -1 and 1 and increase monotonically with ω. Fig. 10(b) visualizes the Pareto-optimal solutions in the A_{total}–$(KA)_{sys}$ space, with color mapping corresponding to different ω values. As ω increases, solutions shift toward lower-area but lower-performance configurations, reflecting increased weight on minimizing A_{total}. For $\omega > 0.8$, A_{total} stabilizes, whereas $0.4 < \omega < 0.75$ yields clustered solutions, revealing a sensitive trade-off region. This trend aligns with the results in Fig. 8. The Pareto front reveals a nonlinear trade-off between A_{total} and $(KA)_{sys}$, offering a continuous and tunable set of optimal solutions for ICHE system design. This facilitates flexible system selection under varying design constraints and performance preferences. Fig. 11 illustrates the thermodynamic parameter distribution of the intermediate fluid along the Pareto front. Red-shaded regions denote mass-oriented configurations, while blue regions emphasize the enhancement of system heat transfer capability. The figure provides a visual framework for selecting optimal intermediate fluid parameters under Table 2 conditions, improving engineering efficiency and guiding coordinated optimization design of ICHE systems.

NSGA-II is a widely adopted genetic algorithm for multi-objective optimization problems. The scalarization method in Section 3.2 may limit Pareto-optimal solutions due to discrete ω values, which may inadequately represent the Pareto front. To overcome this, NSGA-II is applied using the Table 2 operating condition and the structural parameters from Table 3. Both methods' Pareto fronts are compared to ensure the accuracy and completeness of the coordinated optimization design for the ICHE system. NSGA-II is implemented in MATLAB R2021b with a population size of 200, a tolerance of 10^{-6}, and a Pareto fraction of 0.4. Scattered crossover with a crossover rate of 0.8 and Gaussian mutation are employed.

Fig. 12 displays the Pareto front for ICHE system design optimization via the NSGA-II algorithm. The red point set indicates the initial population, while the Pareto front forms the nondominated optimal boundary in the two-objective function space. Notably, the Pareto front in Fig. 12 is identical to that in Fig. 10(b), derived via the scalarization method. This confirms that the Fig. 10(b) solutions are a subset of Fig. 12, constrained by the discrete and finite values of ω. This consistency

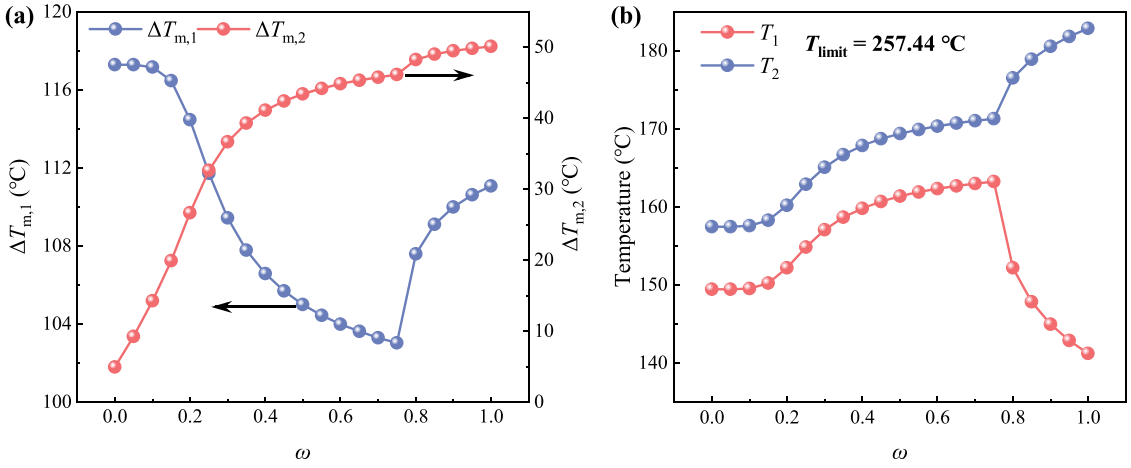

Fig. 9. Effect of weighting factor ω on (a) mean temperature difference; (b) intermediate working fluid temperature.

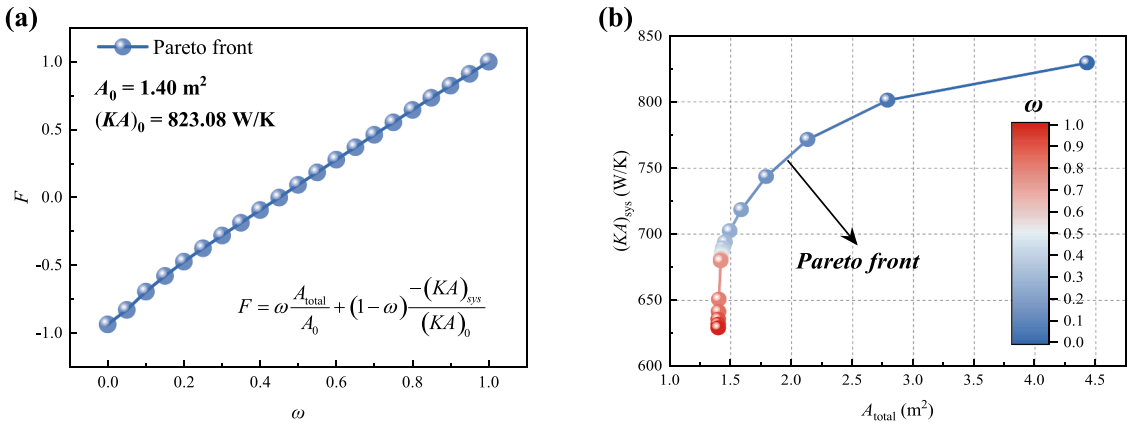

Fig. 10. Pareto front of the basic ICHE system design optimization. (a) Distribution of F; (b) Distribution of A_{total} and $(KA)_{sys}$.

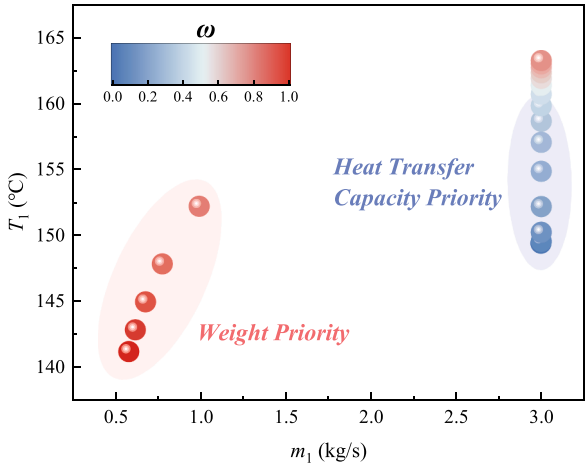

Fig. 11. Distribution of intermediate working fluid thermodynamic parameters corresponding to the Pareto front.

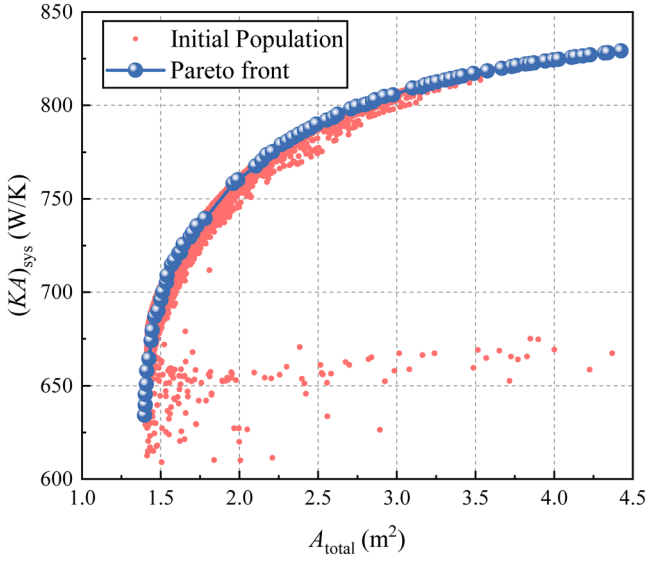

Fig. 12. Pareto front of the basic ICHE system design optimization obtained from the NSGA-II.

demonstrates the mathematical equivalence of the two optimization approaches and further validates the accuracy and reliability of the ICHE system design optimization model developed in this study. The distribution of A_{total} and $(KA)_{sys}$ corresponding to the Pareto front as functions of the intermediate fluid thermodynamic parameters (m_1, T_1) is shown in Fig. 13. The results indicate that the range of m_1 values associated with the Pareto front is relatively broad, spanning [0.65, 3] kg/s, reflecting flexibility in mass flow rate design for the ICHE system. In contrast, the corresponding T_1 values are narrowly concentrated within the range [144, 154] °C, showing greater sensitivity due to tighter thermodynamic constraints. As illustrated in Fig. 7, the narrow feasible range for T_1 is associated with the fact that the optimum occurs near the variable boundary, where the objective function F shows steep gradients. This behavior originates from the LMTD: small variations in T_1 can cause large changes in LMTD, which in turn drive sharp variations in the required heat transfer area and the equivalent conductance KA. In contrast, the optimal range for m_1 is wider, as its influence on LMTD is less direct. Similar sensitivity phenomena were analyzed in detail in our earlier study on ICHE heat transfer area optimization [25], and the results presented here are consistent with that finding. Further analysis reveals a locally concentrated distribution of Pareto-optimal solutions within the interval 2.80 kg/s $< m_1 <$ 2.95 kg/s and 149.0 °C $< T_1 <$ 149.5 °C, accompanied by pronounced variations in A_{total}. It suggests proximity to nonlinear constraint boundaries, making the mean temperature difference in HEXs highly sensitive to perturbations. Overall, Fig. 13 clarifies feasible domains and sensitivities, enhancing the Pareto front's value in guiding ICHE system design.

4.2. *Operational optimization for multi-branch ICHE system*

An operational optimization study was conducted on the multi-branch ICHE system shown in Fig. 2(a), aiming to maximize the system heat transfer rate Q_3 by adjusting the intermediate working fluid mass flow rate ($m_{w,3}$) and the flow distribution ratio (ζ). Before optimization, a steady-state thermodynamic experiment was carried out for the multi-branch ICHE system, as detailed in our previous study [15]. In this section, the accuracy of the system thermal parameters solving module—developed by integrating the HEX heat transfer model with the system transfer matrix-based modeling approach—will first be validated through comparison with experimental data. On this basis, the operational optimization of the multi-branch ICHE system will be carried out using the model described in Section 3.3 to demonstrate the resulting improvements in system performance.

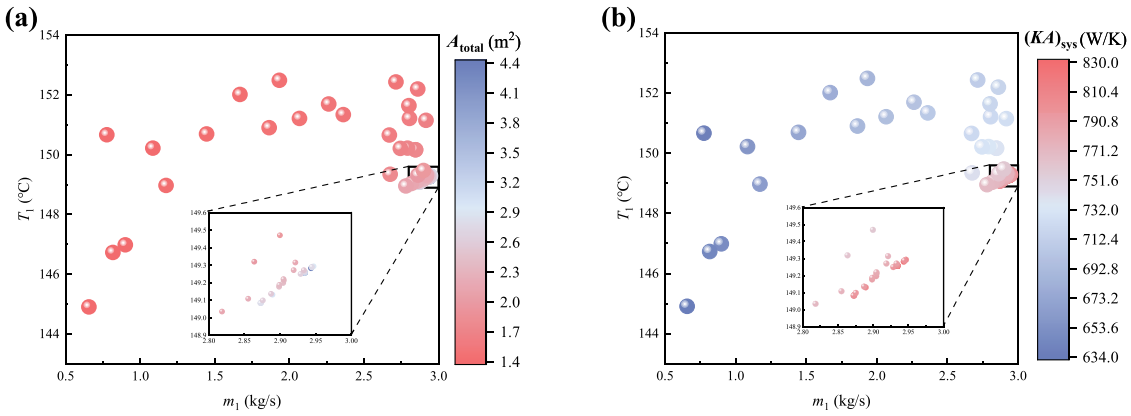

Fig. 13. Distribution of (a) A_{total}; (b) $(KA)_{sys}$ corresponding to the Pareto front as functions of (m_1, T_1).

To identify the K of each HEX under different operating conditions within the system, the coefficient in Eq. (2) must first be determined. Since both HEX-1 and HEX-2 are tube-bundle structures with the intermediate working fluid (water) flowing inside the tubes, the coefficient values for internal flow heat transfer are given by Eq. (3), while external air-side convective heat transfer coefficients are obtained using the Zhukauskas correlation [47]. HEX-3 is an airfoil-type PCHE, for which empirical correlations fitted by Liu et al. based on water [58] and hydrocarbon fuel [45] flow and heat transfer experiments are used, as given below:

$$Nu_{water} = 0.000135 Re_{water}^{1.8978} Pr_{water}^{1/3} \tag{40}$$

$$Nu_{fuel} = 0.07294 Re_{fuel}^{0.6452} Pr_{fuel}^{1/3} \tag{41}$$

Fig. 14 presents the comparison between the calculated results from the thermal parameters solving module and the experimental data for the multi-branch ICHE system, including the heat transfer rates, inlet, and outlet temperatures of each HEX. For any given thermal parameter, at least 88.4% of the experimental data fall within a ±15% deviation band, fully demonstrating the accuracy and robustness of the model.

The hybrid optimization algorithm developed for multi-branch ICHE system operation (Fig. 4) was applied to determine optimal $m_{w,3}$ and ζ. The intermediate fluid's thermodynamic parameter ranges are defined

Table 5
Experimental parameters for operational optimization of multi-branch ICHE system.

Parameter	Value	Parameter	Value
T_7 (°C)	250.34	$P_{w,3,in}$ (MPa)	2.594
T_9 (°C)	224.94	$m_{a,1}$ (kg/s)	0.162
T_{11} (°C)	39.24	$m_{a,2}$ (kg/s)	0.070
$P_{a,1,in}$ (MPa)	0.101	m_f (kg/s)	0.195
$P_{a,2,in}$ (MPa)	0.111	$m_{w,3}$ (kg/s)	0.365
$P_{f,in}$ (MPa)	3.071	ζ	0.606

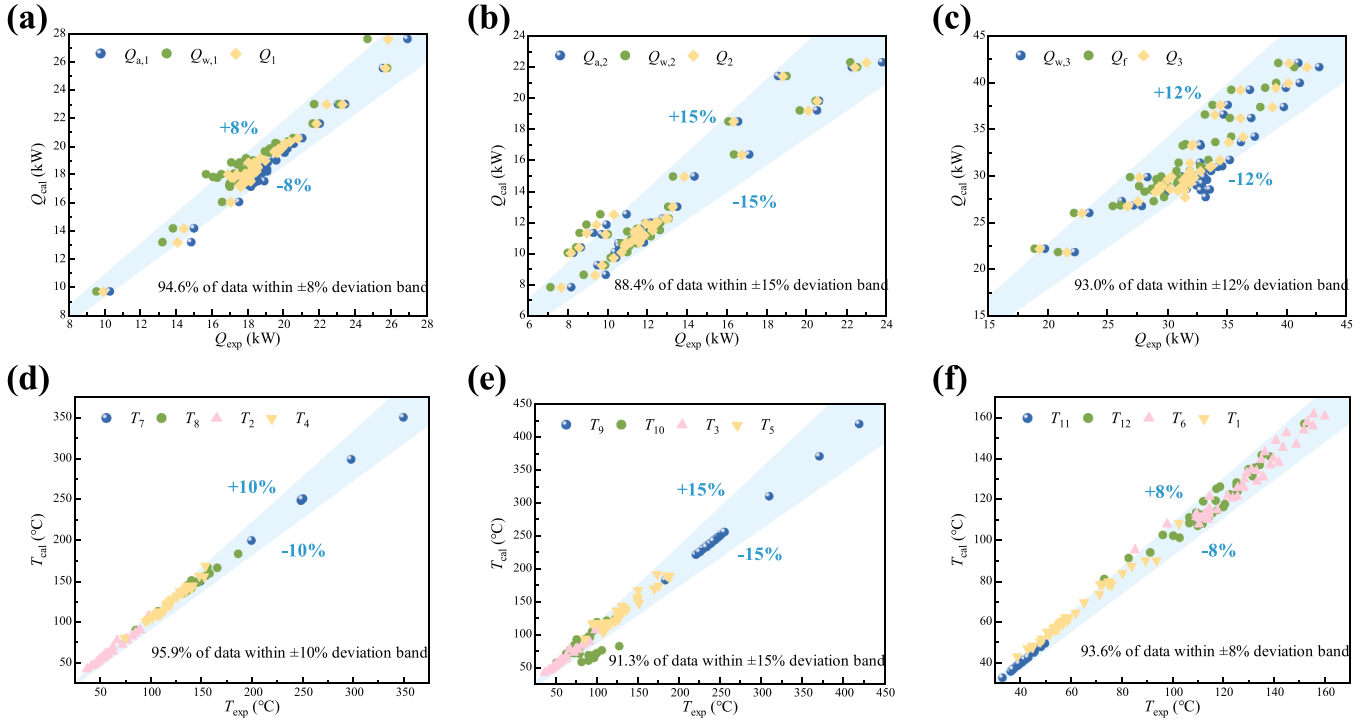

Fig. 14. Comparison between the calculated results of the thermal parameters solving module and experimental data for the multi-branch ICHE system. (a) HEX-1 heat transfer rates; (b) HEX-2 heat transfer rates; (c) HEX-3 heat transfer rates; (d) HEX-1 inlet and outlet temperatures; (e) HEX-2 inlet and outlet temperatures; (f) HEX-3 inlet and outlet temperatures.

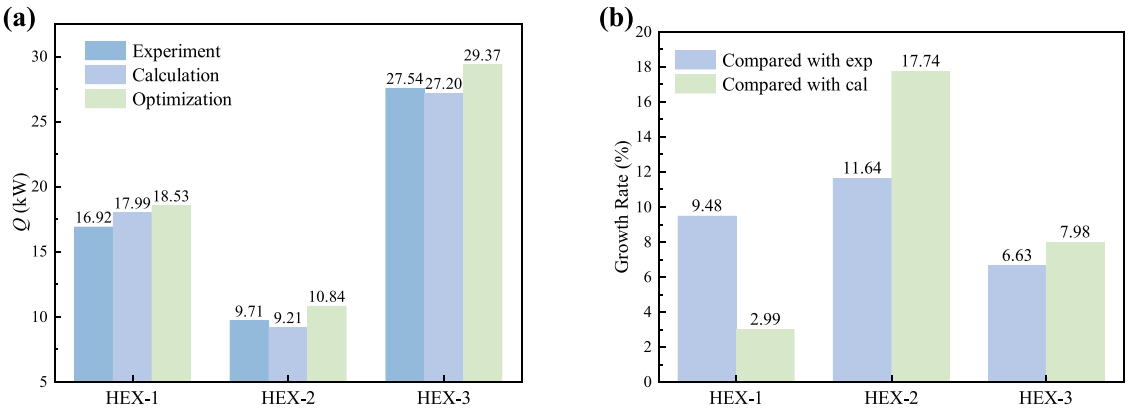

Fig. 15. (a) Comparison of heat transfer rates for each HEX before and after optimization; (b) Growth rates of heat transfer rates after optimization relative to experimental data and thermal parameters solving model calculation results.

Table 6
Thermal parameters values before and after optimization.

	Experimental value	Calculation value	Optimization Value
$m_{w,3}$ (kg/s)	0.365	0.365	0.090
ζ	0.606	0.606	0.667
Q_1 (kW)	16.92	17.99	18.53
Q_2 (kW)	9.71	9.21	10.84
Q_3 (kW)	27.54	27.20	29.37
T_1 (°C)	93.68	90.36	53.30
T_2 (°C)	91.30	90.36	53.30
T_3 (°C)	91.50	90.36	53.30
T_4 (°C)	108.19	109.68	127.00
T_5 (°C)	107.85	105.56	139.56
T_6 (°C)	110.72	108.06	131.19
T_8 (°C)	141.32	142.16	139.08
T_{10} (°C)	92.32	96.56	73.70
T_{12} (°C)	109.93	107.28	112.33

as $m_{w,3} \in [0.01, 1.5]$kg/s, $\zeta \in [0.4, 0.9]$. Given that experimental uncertainty may influence quantitative comparisons, a comparative analysis was conducted for the representative condition in Table 5, as illustrated in Fig. 15. The analysis compares experimental data, thermal parameters solving model calculations, and optimization results. Table 6 lists the thermal parameter values before and after optimization. Fig. 15(a) shows that deviations between experimental results and the thermal parameter solving model calculations are minor, with differences less than 1.07 kW, further validating the operational optimization model. Under the given condition, optimizing the intermediate fluid mass flow rate and distribution ratio improved heat transfer in all HEXs. Specifically, compared to the experimental results, the heat transfer rates of HEX-1, HEX-2, and HEX-3 increased by 9.48%, 11.64%, and 6.63%, respectively. While compared to the calculation results, the heat transfer rates of HEX-1, HEX-2, and HEX-3 increased by 2.99%, 17.74%, and 7.98%, respectively. Although the developed optimization model does not explicitly account for heat losses, Fig. 15 compares the optimization results with both the calculation model (neglecting heat losses) and the experimental data, showing that the growth rates obtained by optimization relative to the calculation baseline closely match those relative to the experiments. This consistency confirms that the improvements originate from the optimization itself, and that the neglect of external heat losses does not alter the validity of the conclusions. These improvements suggest deeper utilization of engine energy in practical aero engine operation. With thermal constraints met, the enhanced recovery of waste heat contributes to improving the engine's thermal efficiency.

Notably, after optimization, $m_{w,3}$ decreased markedly from 0.365 kg/s to 0.090 kg/s, which appears counterintuitive. For a single HEX, increasing the working fluid mass flow rate generally enhances heat transfer by raising *Re* and HEX's thermal conductance *KA*. However, in ICHE systems, the dominant factor influencing system-level heat transfer is the average heat transfer temperature difference, rather than *KA*. While *KA* represents the reciprocal of the total thermal resistance, it is limited by the side with the greater thermal resistance. In the multi-branch ICHE system operational optimization, only the intermediate fluid mass flow rate is adjusted, while the inlet temperatures and mass flow rates of the other working fluids remain fixed, leaving their resistance unchanged. Thus, even if $m_{w,3}$ increases and reduces internal resistance, *KA* remains limited by the fixed side. In contrast, varying $m_{w,3}$ or ζ can markedly shift mean temperature differences across each HEX. For instance, decreasing $m_{w,3}$ can raise mean temperature differences significantly, exerting a stronger influence. Hence, the mean temperature difference—not *KA*—serves as the key determinant of heat transfer rate enhancement in multi-branch ICHE system optimization. Fig. 16 presents a comparison of the *KA* and LMTD for each HEX before and after optimization under the operating condition specified in Table 5. It can be observed that after optimization, $(KA)_1$ and $(KA)_2$ exhibit slight decreases, while $(KA)_3$ shows a significant reduction. In contrast, the LMTD values for all HEXs increase markedly. These results validate the aforementioned analysis.

Under the operating condition specified in Table 5, we investigated the individual impact of $m_{w,3}$ and ζ on the optimization results. Specifically, we performed separate optimizations by fixing either ζ or $m_{w,3}$, with the corresponding thermal parameters before and after optimization summarized in Table 7. When optimizing with $m_{w,3}$ as the sole variable, $m_{w,3}$ was significantly reduced, and Q_3 was still substantially enhanced. This 7.69% increase in Q_3 closely approached the 7.98% gain from the joint optimization of $m_{w,3}$ and ζ. However, optimizing ζ alone yielded only a 0.30% increase in Q_3, indicating that under this condition, $m_{w,3}$ serves as the primary control variable. In summary, the operational optimization of the multi-branch ICHE system should involve the simultaneous adjustment of $m_{w,3}$ and ζ to achieve optimal performance, with $m_{w,3}$ exerting a more significant influence than ζ.

It is worth noting that the operational optimization model introduced in Section 3.3 is essentially aimed at addressing system performance under off-design conditions. The representative case analyzed in this section demonstrates that, if the ICHE system operates without adjustment of $m_{w,3}$ and ζ, it remains stable but the heat transfer rate Q_3 falls below the achievable optimum. By actively regulating these parameters, the system recovers part of the lost performance—for example, an improvement of up to 7.98% in Q_3 was obtained in the tested case. At some operating points, however, the improvement is smaller, which reflects the limited admissible variation of $m_{w,3}$ and ζ and the fact that the baseline may already be close to the optimal region. These results indicate that the proposed operational optimization not only enhances performance at the design point but also provides adaptability under varying loads, thereby ensuring robust thermal

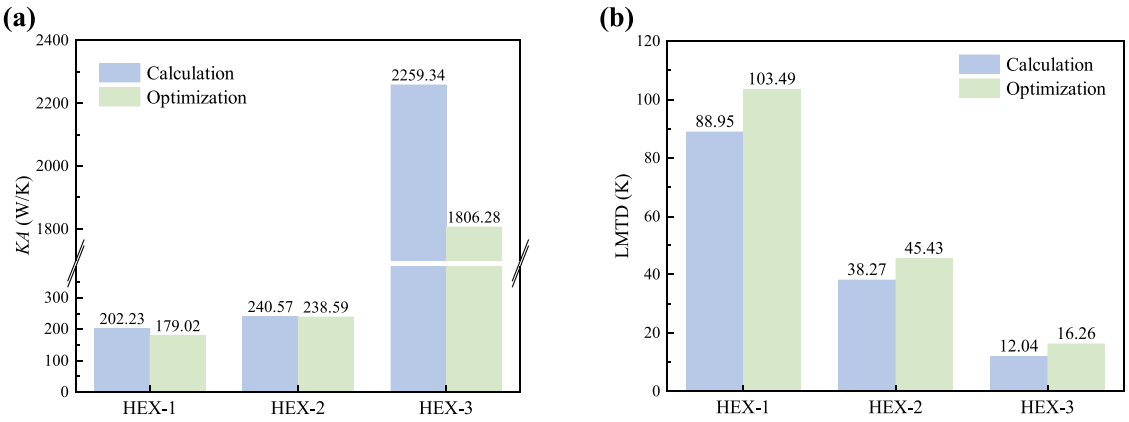

Fig. 16. Comparison of (a) *KA* and (b) LMTD for each HEX before and after optimization.

Table 7
Individual impact of $m_{w,3}$ and ζ on the optimization results.

	Calculation value	Change $m_{w,3}$ Optimization Value	Change ζ Optimization Value
$m_{w,3}$ (kg/s)	0.365	0.0893	0.365
ζ	0.606	0.606	0.763
Q_1 (kW)	17.99	18.23	18.17
Q_2 (kW)	9.21	11.06	9.11
Q_3 (kW)	27.20	29.29	27.28
Q_3 growth rate	/	7.69%	0.30%

performance across a broader operating envelope.

In addition to improving overall heat transfer performance, the ICHE scheme also contributes to fuel coking mitigation. Although direct wall temperatures were not measured in the present experiments, they can be estimated from bulk fluid temperatures, mass flow rates, convective heat transfer coefficients, and known heat transfer areas. A comparative evaluation performed under a representative engine condition indicated that, for Chinese aviation kerosene RP-3, the ICHE configuration lowers the maximum fuel wall temperature by about 40 °C relative to a direct fuel–air heat exchange layout. Given that oxidative coking of aviation kerosene typically initiates around 150 °C and the deposition rate peaks near 316 °C [59], this reduction provides a significant margin against coking and illustrates an important operational advantage of the ICHE system.

5. Conclusions

In this study, a full-process optimization framework for intermediate cycle heat exchange (ICHE) systems in aero engines is developed, covering both design-stage trade-off analysis and operational performance enhancement. The approach combines multi-objective optimization, energy-flow modeling, and experimental validation to address the coupled challenges of thermal efficiency, system weight, and adaptability to variable working conditions. The main conclusions are as follows:

(i) A coordinated design model was proposed with the total heat transfer area and system equivalent heat conductance as dual objectives, and a hybrid optimization algorithm was developed to solve it. The accuracy of the design optimization model was verified through exhaustive calculation, with a maximum relative deviation of 0.13%.

(ii) The necessary condition for optimality in ICHE system design optimization was derived (as shown in Eq. (25)), revealing that Pareto-optimal solutions satisfy the gradient collinearity condition. A visual mapping framework for selecting optimal intermediate fluid parameters under typical operating conditions was provided, offering clear guidance for the design optimization of the ICHE system.

(iii) The operational optimization model for the multi-branch ICHE system was proposed. An integrated thermal parameter solving method combining the HEX heat transfer model with the system transfer matrix-based model was developed, and its accuracy and robustness were validated through experiments, with over 88.4% of the experimental data falling within a ±15% deviation.

(iv) For multi-branch ICHE system operational optimization, joint adjustment of the intermediate fluid mass flow rate and its distribution among branches yields a 7.98% improvement in system heat transfer rate, with the mean temperature difference identified as the dominant performance driver.

CRediT authorship contribution statement

Weitong Liu: Writing – original draft, Software, Methodology, Investigation, Formal analysis, Data curation. **Guoqiang Xu:** Supervision, Conceptualization. **Yiang Liu:** Resources. **Xiuting Gu:** Resources. **Jiayang Wang:** Resources. **Jingzhi Zhang:** Writing – review & editing. **Yanchen Fu:** Writing – review & editing, Project administration, Funding acquisition.

Declaration of competing interest

The authors declare that they have no known competing financial interests or personal relationships that could have appeared to influence the work reported in this paper.

Acknowledgment

The authors appreciate the supports from the Beijing Nova Program (No. 20240484560), Beijing Municipal Science & Technology Commission, Administrative Commission of Zhongguancun Science Park (No. Z241100007424005), and the Academic Excellence Foundation of BUAA for PhD Students.

Data availability

Data will be made available on request.

References

[1] A.S.J. van Heerden, D.M. Judt, S. Jafari, C.P. Lawson, T. Nikolaidis, D. Bosak, Aircraft thermal management: practices, technology, system architectures, future challenges, and opportunities, Prog. Aerosp. Sci. 128 (2022).
[2] S. Zhang, X. Li, J. Zuo, J. Qin, K. Cheng, Y. Feng, et al., Research progress on active thermal protection for hypersonic vehicles, Prog. Aerosp. Sci. (2020) 119.

[3] C. Dang, J. Xu, Z. Chen, K. Cheng, J. Qin, G. Liu, Comparative study of different layouts in the closed-Brayton-cycle-based segmented cooling thermal management system for scramjets, Energy 301 (2024).
[4] L. Zhang, C. Wang, P. Yan, J. Fang, X. Xiu, J. Qin, et al., Performance analysis of a new precooled engine cycle based on the combined pre-compressor cooling with mass injection and heat exchanger, Energy Convers. Manag. 322 (2024).
[5] G.B. Bruening, WS. Chang, Cooled Cooling Air Systems For Turbine Thermal management. Turbo Expo: Power for Land, Sea, and Air, American Society of Mechanical Engineers, 1999, p. V003T01A2.
[6] Y. Fu, W. Liu, J. Wang, L. Zhang, J. Wen, H. Wu, et al., Experimental investigation on heat transfer enhancement of supercritical pressure aviation kerosene in tubular laminar flow by vibration, Appl. Therm. Eng. (2024) 257.
[7] Rolt AM, Kyprianidis K. Assessment of new aero engine core concepts and technologies in the EU framework 6 NEWAC programme. ICAS 2010 Congress Proceedings, Paper No 4082010.
[8] M. Chen, J. Zhang, H. Tang, Performance analysis of a three-stream adaptive cycle engine during throttling, Int. J. Aerosp. Eng. 2018 (2018).
[9] Chepkin V. New generation of russian aircraft engines conversion and future goals. Proc of the International Symposium on Air Breathing Engines 1999.
[10] Y. Fu, H. Zhi, J. Wang, J. Sun, J. Wen, G. Xu, Numerical Research On Heat Transfer and Thermal Oxidation Coking Characteristics of Aviation Kerosene RP-3 Under Supercritical Pressure, International Communications in Heat and Mass Transfer, 2024, p. 159.
[11] H.W. Deng, K. Zhu, G.Q. Xu, Z. Tao, C.B. Zhang, GZ. Liu, Isobaric specific heat capacity measurement for kerosene RP-3 in the near-Ccitical and supercritical regions, J. Chem. Eng. Data 57 (2011) 263–268.
[12] N.R. Herring, SD. Heister, Review of the development of compact, high performance heat exchangers for gas turbine applications, ASME Int. Mech. Eng. Congr. Expo. (2006) 467–476.
[13] Y. Liu, G. Xu, Y. Fu, J. Wen, H. Huang, Thermal dynamic and failure research on an air-fuel heat exchanger for aero-engine cooling, Case Stud. Therm. Eng. (2023) 42.
[14] W. Liu, G. Xu, X. Gang, H. Qi, M. Li, J. Wen, et al., Theoretical modeling, experimental validation, and thermodynamic analysis on intermediate heat-exchange cycle system, Int. Commun. Heat Mass Transf. 156 (2024).
[15] W. Liu, G. Xu, X. Gu, J. Yao, M. Li, M. Lei, et al., Experimental analysis and thermodynamic modeling for multilevel heat exchange system with multifluid in aero engines, Energy (2025) 315.
[16] M. Noton, G. Swinerd, Optimization of the rocket-powered ascent of HOTOL, Acta Astronaut. 19 (1989) 17–26.
[17] R. Aggarwal, K. Lakhara, P. Sharma, T. Darang, N. Jain, S. Gangly, SABRE ENGINE: single stage to orbit rocket engine, Int. J. Innov. Res. Sci. Eng. Technol. 4 (2015) 10360–10366.
[18] J. Zhang, Z. Wang, Q. Li, Thermodynamic efficiency analysis and cycle optimization of deeply precooled combined cycle engine in the air-breathing mode, Acta Astronaut. 138 (2017) 394–406.
[19] Longstaff R, Bond A. The Skylon project. 17th AIAA International Space Planes and Hypersonic Systems and Technologies Conference 2011. p. 2244.
[20] Zhou J, Lu H, Zhang H, Zhao L, Chen J, Zheng R. A preliminary research on a two-stage-to-orbit vehicle with airbreathing pre-cooled hypersonic engines. 21st AIAA International Space Planes and Hypersonics Technologies Conference 2017.
[21] C. Wang, X. Yu, X. Pan, J. Qin, H. Huang, Thermodynamic optimization of the indirect precooled engine cycle using the method of cascade utilization of cold sources, Energy (2022) 238.
[22] J. Liu, S. Wang, T. Zhang, Y. Wang, K. He, Z. Cui, et al., Experiment and simulation on a thermal management scheme of intermediate circulation based on heat current method, Int. J. Heat Mass Transf. (2023) 206.
[23] E.Y.M. Ang, P.S. Ng, C.B. Soh, PC. Wang, Multi-stage thermoelectric coolers for cooling wearables, Therm. Sci. Eng. Prog. (2022) 36.
[24] Z. Zhang, Z. Wu, X. Luo, W. Liu, Numerical study on convective heat transfer of liquid metal gallium in turbine guide vane, Aerospace 10 (2023).
[25] Y. Fu, W. Liu, H. Qi, Q. Chen, J. Wen, G. Xu, Heat transfer area optimization of intermediate heat-exchange cycle system for aero engines, Int. J. Heat Mass Transf. 220 (2024).
[26] J. Liu, M. Li, T. Zhang, Y. Wang, Z. Cao, W. Shao, et al., Optimization of the aero-engine thermal management system with intermediate cycle based on heat current method, Appl. Therm. Eng. 237 (2024).
[27] J. Wen, C. Wan, G. Xu, L. Zhuang, B. Dong, J. Chen, Optimization of thermal management system architecture in hydrogen engine employing improved genetic algorithm, Energy (2024) 297.
[28] J. Sarkar, S. Bhattacharyya, Overall conductance and heat transfer area minimization of refrigerators and heat pumps with finite heat reservoirs, Energy Convers. Manag. 48 (2007) 803–808.
[29] L. Chen, F. Sun, C. Wu, Optimal allocation of heat-exchanger area for refrigeration and air-conditioning plants, Appl. Energy 77 (2004) 339–354.
[30] L. Zhuang, G. Xu, Q. Liu, M. Li, B. Dong, J. Wen, Superiority analysis of the cooled cooling air technology for low bypass ratio aero-engine under typical flight mission, Energy Convers. Manag. (2022) 259.
[31] T. Jiang, T-T Zhan, Y-H Li, K. Yang, N. He, N. Wang, et al., Heat transfer characteristics and flow distribution behavior of pyrolytic ammonia in scramjet regenerative cooling channels, Energy 335 (2025).
[32] P. Liu, T. Yang, H. Zheng, X. Huang, X. Wang, T. Qiu, et al., Thermodynamic analysis of power generation thermal management system for heat and cold exergy utilization from liquid hydrogen-fueled turbojet engine, Appl. Energy (2024) 365.
[33] P. Rašković, S. Stoiljković, Pinch design method in the case of a limited number of process streams, Energy 34 (2009) 593–612.
[34] PV. Coveney, The second law of thermodynamics: entropy, irreversibility and dynamics, Nature 333 (1988) 409–415.
[35] M. Kalinin, S. Kononogov, Boltzmann's constant, the energy meaning of temperature, and thermodynamic irreversibility, Meas. Tech. 48 (2005) 632–636.
[36] A. Bejan, Entropy generation minimization: the new thermodynamics of finite-size devices and finite-time processes, J. Appl. Phys. 79 (1996) 1191–1218.
[37] A. Bejan, Method of entropy generation minimization, or modeling and optimization based on combined heat transfer and thermodynamics, Revue Générale de Thermique 35 (1996) 637–646.
[38] Klein S, Reindl D. The relationship of optimum heat exchanger allocation and minimum entropy generation rate for refrigeration cycles. 1998.
[39] O. Balli, E. Ozbek, S. Ekici, A. Midilli, T. Hikmet Karakoc, Thermodynamic comparison of TF33 turbofan engine fueled by hydrogen in benchmark with kerosene, Fuel 306 (2021).
[40] G. Tsatsaronis, Strengths and Limitations of Exergy analysis. Thermodynamic optimization of Complex Energy Systems, Springer, 1999, pp. 93–100.
[41] Q. Chen, J. Hao, T. Zhao, An alternative energy flow model for analysis and optimization of heat transfer systems, Int. J. Heat Mass Transf. 108 (2017) 712–720.
[42] T. Zhao, X. Chen, K-L He, Q. Chen, A standardized modeling strategy for heat current method-based analysis and simulation of thermal systems, Energy (2021) 217.
[43] D. Liu, Q. Chen, K.L. He, X. Chen, An integrated system-level and component-level optimization of heat transfer systems based on the heat current method, Int. J. Heat Mass Transf. 131 (2019) 623–632.
[44] Y. Liu, G. Xu, Y. Fu, J. Wen, S. Qi, L. Lyu, Airside pressure drop characteristics of three analogous serpentine tube heat exchangers considering heat transfer for aero-engine cooling, Chin. J. Aeronaut. 35 (2022) 32–46.
[45] W. Liu, G. Xu, H. Zhi, R. Wang, M. Li, Y. Fu, Experimental evaluation of hydrothermal performance in airfoil-fin pche with supercritical pressure hydrocarbon fuel, Int. Commun. Heat Mass Transf. (2024) 159.
[46] A. Bejan, Convection Heat Transfer, John wiley & sons, 2013.
[47] K. Thulukkanam, Heat Exchanger Design Handbook, CRC press, 2013.
[48] The MathWorks Inc. MATLAB version: 9.11.0 (R2021b), The MathWorks Inc., Natick, Massachusetts, 2021.
[49] M.H. Ahmadi, MA. Ahmadi, Multi objective optimization of performance of three-heat-source irreversible refrigerators based algorithm NSGAII, Renew Sustain. Energy Rev. 60 (2016) 784–794.
[50] K. He, T. Zhao, Q. Chen, X. Chen, Matrix-based network heat transfer modeling approach and its application in thermal system analysis, Appl. Therm. Eng. (2020) 181.
[51] T. Zhao, Q. Sun, X. Li, Y. Xin, Q. Chen, A novel transfer matrix-based method for steady-state modeling and analysis of thermal systems, Energy (2023) 281.
[52] I.H. Bell, J. Wronski, S. Quoilin, V. Lemort, Pure and pseudo-pure fluid thermophysical property evaluation and the open-source thermophysical property library coolprop, Ind. Eng. Chem. Res. 53 (2014) 2498–2508.
[53] Y. Fu, W. Liu, S. Shi, R. Wang, Y. Liu, G. Xu, Density measurements of aviation kerosene RP-3 over temperature range from 323 K to 783 K under supercritical pressures from 6 MPa to 8 MPa, Chin. J. Aeronaut. 38 (2025).
[54] Y. Liu, G. Xu, S. Shi, R. Wang, Y. Fu, Viscosity measurements of endothermic propellant ehf-tu and aviation kerosene RP-3 under supercritical pressures, J. Chem. Eng. Data 70 (2025) 827–834.
[55] G.Q. Xu, Z.X. Jia, J. Wen, H.W. Deng, YC. Fu, Thermal-Conductivity measurements of aviation kerosene RP-3 from (285 to 513) K at Sub- and Supercritical pressures, Int. J. Thermophys. 36 (2015) 620–632.
[56] T. Jia, Q. Liu, J-J Zou, X. Zhang, L. Pan, The dynamics and mechanism of JP-10 thermal oxidative deposition, Fuel (2022) 321.
[57] Z.H. Sander, Z.J. West, J.S. Ervin, S. Zabarnick, Experimental and modeling studies of heat transfer, fluid dynamics, and autoxidation chemistry in the jet fuel thermal oxidation tester (JFTOT), Energ Fuel 29 (2015) 7036–7047.
[58] W. Liu, H. Zhi, H. Qi, Y. Fu, Experimental insights into thermal-hydraulic performance of a compact printed circuit heat exchanger with airfoil fins using high-pressure water, in: International Conference on Micro/Nanoscale Heat Transfer, American Society of Mechanical Engineers, 2024 p. V001T09A.
[59] L. Spadaccini, D. Sobel, H. Huang, Deposit formation and mitigation in aircraft fuels, J. Eng. Gas Turbines Power 123 (2001) 741–746.